THE EFFECTS OF TOWFISH MOTION ON SIDESCAN SONAR IMAGES

(2)

S.D. ANSTEE

AR-006-622

MRL-RR-1-94

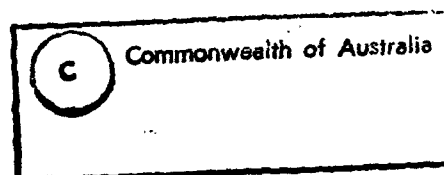FEBRUARY 1994

AD-A279 252

DTIC
S ELECTE
MAY 1 7 1994
F D

APPROVED

FOR PUBLIC RELEASE

O

C Commonwealth of Australia

MATERIALS RESEARCH LABORATORY

DSTO

The Effects of Towfish Motion on Sidescan Sonar Images

S.D. Anstee

MRL Research Report
MRL-RR-1-94

Abstract

A simulation algorithm to estimate the geometrical effects of towfish motions on sidescan sonar images is described. The results of simulations using the algorithm are discussed, and bounds for acceptable amplitudes of towfish motions are estimated. Yaw is found to be the most potentially damaging towfish motion, and a sinusoidal yaw motion with amplitude 0.5° and period 3 s is found to induce unacceptable distortion of a towfish image. The effects of towfish motions on the coverage of the seabed are also discussed.

DTIC QUALITY INSPECTED 8

94-14601

DEPARTMENT OF DEFENCE
DSTO MATERIALS RESEARCH LABORATORY

94 5 16 048

Author

Stuart Anstee

Dr Anstee is a Research Scientist in the Maritime Operations Division at MRL Sydney. He joined DSTO in 1988 as a Cadet Research Scientist and obtained a PhD in atomic physics at Queensland University in 1992. His present research interests are in various aspects of sonar performance.

Contents

The Effects of Towfish Motion on Sidescan Sonar Images

1. Introduction

Images from sidescan sonars are well known to be adversely affected by transducer motions during sidescan operation. In some operating conditions, the images can be distorted sufficiently that objects on the sea floor can be overlooked or obscured beyond recognition. The purpose of this report is to give an estimation of the amounts and types of transducer motions which cause significant image degradation.

The particular sidescan sonar dealt with in this work is the Klein Associates 595 system with the 422S-101HF dual-frequency "100-500" kHz towfish currently employed by the RAN in a route survey and mine sweeping capacity.

The *towfish* is a torpedo-shaped towed body with unfocussed linear transducer packages mounted symmetrically on both sides. The transducer packages simultaneously output beams at approximately 100 and 400 kHz, on both sides of the towfish. All four beams are directed perpendicular to the towing direction (the *across-track* direction) and are very narrow in the towing or *along-track* direction. The dual-frequency operation effectively provides two different resolution images of the same area of the seabed. In this report, each frequency is considered separately and the conclusions of the report should be applicable to most similar single-beam sidescan sonars operating at comparable frequencies.

Since the transducer packages are usually mounted in a towfish, transducer motion fluctuations will be referred to in this report as *towfish motions*. In the absence of towfish motions, the towfish follows a straight, level *tow path* at uniform velocity.

During normal sidescan sonar operation, the towfish is towed behind a ship by a length of cable which serves to control the working depth of the towfish and to isolate the towfish somewhat from the motions of the ship. In spite of the cable, the towfish is perturbed both by ship motions and by motions of the water body, causing its position and orientation to fluctuate.

In order to investigate the effects of towfish motions, a numerical model, described below, was used to simulate the images expected from the Klein sidescan sonar during particular motions. The images allowed a subjective evaluation of the effects of the motions, and gave an indication of the limits to acceptable motions. Most of the images from the simulations involved minelike

objects, and some representative examples of such images are included in this report.

Towfish motions were modelled by sinusoidal variations with periods similar to the cycle times of typical ship and wave motions. Each of the three translations and three rotations was treated separately.

Additional calculations were made based on simpler analytical models, so as to check the simulations for the most important motions. Some use of outputs from the simulations was also made to estimate the probability that a given sidescan run could completely fail to detect ("miss") a minelike object. Some results from these calculations are also presented here.

2. The Sidescan Sonar Model

The operation of the sidescan sonar was simplified where possible, retaining only those aspects of the device which are most relevant to the effects of towfish motion on images. In particular, the effects of motions on the imaging of *targets*, or minelike objects, was considered most important, rather than the imaging of the background. A related topic, the imaging of *shadows* caused by the targets, was not treated in this work, since this would have involved the introduction of several further variables to the problem. In spite of this, the effects of motions on shadows should be of similar magnitude to the effects of motions on targets, since both effects are caused by similar geometry.

Many symbols are introduced in the forthcoming sections. Most of these symbols are defined in Section 10 of this work, in a glossary of terms.

A model of the sidescan sonar involves a model of the towfish and its transducers and beam formers; a model of the sea floor, targets and propagation; and a model of the sidescan data treatment and output.

For later convenience, we define some terms here:

- the *swath* of the sidescan is the coverage of its beams across-track, both sides of the towfish;
- the *range scale* is the distance across-track from the towfish to the edge of the swath, or the operating range of the sidescan;
- the *slant range* of a point on the seabed is the straight-line distance from the towfish to the point;
- the *footprint* of a beam is the pattern of beam directivity function values at the intersection of the beam with the seabed. The footprint moves as the towfish moves, so the beam footprint at the moment of pulse emission is not the same as the beam footprints when echoes return.

2.1 The Towfish

The sonar towfish consists of a long, thin, hollow cylinder with a cable attached to the top of the body via a short arm, long transducer packages mounted symmetrically on either side, a rounded nose and tail fins for stability and an internal electronics package for signal processing.
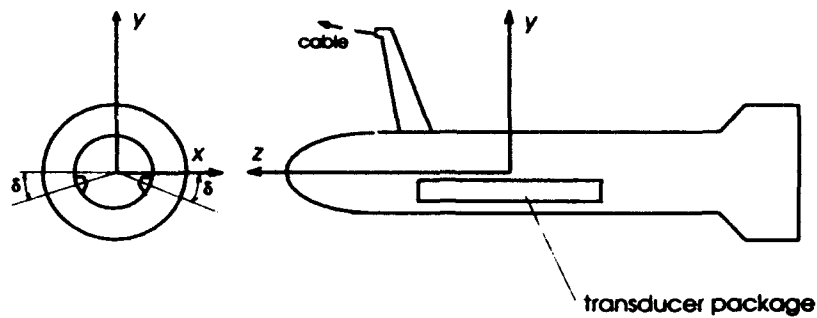
Figure 1: *Front cross-section (left) and side view (right) (not to scale) of a sonar towfish showing the local coordinate system with its origin at the nominal centre of mass. The towfish moves in the positive z-direction. The x-direction is positive to port. The transducers are tilted downward from the horizontal by a depression angle* δ.

Figure 1 shows a diagram of a towfish with the local coordinate system adopted for it, and the position of the transducers. The towfish coordinate system is fixed to the towfish. In the absence of perturbations, the body of the towfish is assumed to be level. The nose of the towfish defines the positive z-direction, the x-direction points to port and the y-direction points to the top of the towfish.

For simplicity, assume that the origin is at the centre of mass of the towfish, and that the transducer packages are symmetrically located with respect to the origin. In fact the centre of mass is forward of the transducer centres, but remains close enough that rotation of the towfish does not result in appreciable motion of the centres of the transducers.

The beams of the transducers are assumed to radiate symmetrically about the x-y plane. The beams are very narrow in the z-direction, but very broad "across-track", in the y-direction. The *depression angle*, δ, as shown in Figure 1, can be set so that the beams are either horizontal (0°), or tilted downward with settings of -10° or -20° relative to the x-z plane.

The diameter of the towfish is less than 10 cm, so that for calculations of slant ranges to the seabed, the beams are treated as emanating from the origin.

2.2 Transducers

The transducer packages for the dual-frequency sonar each contain two separate transducer elements, one for each frequency. Each element is a compound device composed of many separate ceramic elements cemented together. Steel, epoxy and other surrounding materials further complicate the structure. The response and directivity of such a transducer package is difficult to predict with accuracy, but approximate beam profiles are adequate in this model.

Figure 2 shows an approximate view of the starboard dual-frequency transducer package. The elements act as unfocussed apertures, and for the purposes of this work, both elements are considered as perfect two-dimensional rectangular pistons, ignoring their surroundings. It is assumed that both elements have a total length of 470 mm. Klein quote a 40° beamwidth for both elements in the "across-track" direction perpendicular to the long axis, and the width of each element is adjusted to produce this.
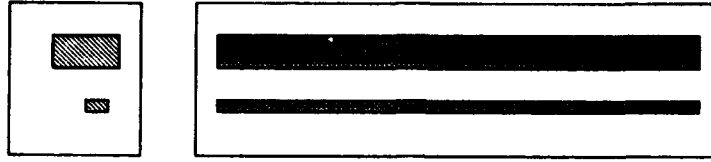
Figure 2: *Approximate cross-section (left) and front view (right) of the starboard transducer package, not to scale. The upper element operates at approximately 100 kHz and the lower element at approximately 400 kHz. Backing materials, matching layers and epoxy surroundings are not shown.*

Both beams are assumed to come from the origin at the centre of the towfish, and to be symmetric about the centre of the transducer package.

2.2.1 Beam Profiles

To emit a pulse, a high-voltage (750 V) electrical pulse is discharged across each transducer element. The resultant ringing of the transducer element at its resonant frequency drives an acoustic pulse which decays after several cycles. The pulses for the two frequencies are emitted slightly apart in time, with the lower frequency emitted approximately 60 μs after the higher frequency, sufficient to separate the two wavetrains in the water, without allowing significant movement of the towfish. After emission, detection circuits connected to the same transducers are used to receive echo returns.

Pulse frequencies of 108 kHz and 380 kHz are assumed in the model, as measured from a particular unit. The frequencies of other units may vary somewhat. For simplicity CW expressions are used for the directivity calculations, which assume unfocussed, rectangular apertures operating as perfect pistons. The pulses are assumed to be so short that range-resolution is unaffected by the pulse-length, but are modelled as single-frequency. It is also assumed that directivities on emission and reception are the same. Experimentally measured beam profiles for a Klein 400 kHz transducer suggest that the above approximations are adequate.

Beam profile calculations are most conveniently made with reference to angular variables. Define the range r, along-track angle κ and across-track angle η of a point of interest, relative to the transducer face, as shown in Figure 3. Define the quantities

$$u = \sin \kappa, \quad v = \sin \eta$$

in terms of the angles η and κ, to be used later in calculations.
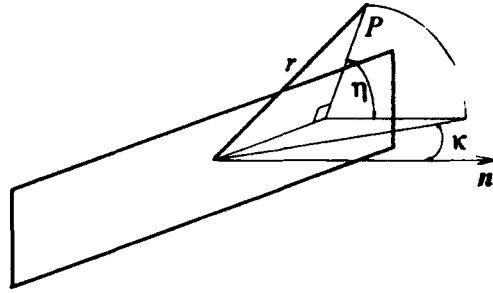
Figure 3: *Along-track angle κ and across-track angle η for a point P, relative to the face of a transducer element and its surface normal n. r is the range from the centre of the element to P. Note that η implicitly depends on the depression angle δ when the transducer is considered as part of the towfish.*

The relationship between the quantities u, v and the local towfish coordinate system (x, y, z) is given at the end of Section 3, and can also be deduced from Figure 1. Note that the angle κ is defined to be positive in the direction of forward motion of the towfish, and the angle η is defined to be positive toward the top of the towfish, regardless of which side of the towfish the transducer is located on.

The directivity function for a rectangular piston can be separated into the product of the directivity functions for two linear apertures at right angles, giving an along-track, *narrow* directivity function due to the length and an across-track *broad* directivity function due to the width of the transducer. Define

$$b(u, v, r) \approx b_n(u, r) b_b(v)$$

where the narrow directivity function is dependent on the range, but the broad directivity function is not, since typical slant ranges to the sea floor lie in the far field of an equivalent linear aperture. (Note that the use of the across-track quantity v in the expression for the broad directivity function is a convenient approximation, which becomes less accurate for points far away from broadside of the towfish, that is, with large values of u. Such points are deemed to lie outside the region of interest for a sidescan sonar.)

The far-field expression for the broad directivity function is

$$b_b(v) \approx \text{sinc}^2\left(\frac{Wv}{\lambda}\right)$$

where W is the transducer width and λ is the wavelength. Klein's figure of 40° for the -3 dB beam width requires a transducer width of approximately 19 mm at 108 kHz and 5 mm at 380 kHz.

In the far field of the long axis of the transducers, the same approximation applies, giving

$$b_n(u, r) \rightarrow b_n(u) \approx \text{sinc}^2\left(\frac{Lu}{\lambda}\right)$$

where L is the length, taken to be 470 mm. The far field of the transducer begins for r greater than approximately 15 m at 108 kHz and 58 m at 380 kHz. In the near field it is more appropriate to use the Fresnel approximation for the linear aperture, (Ziomek, 1985), giving

$$d_n(u,r) = \int_{-L/2}^{L/2} e^{-ikx^2/2r} e^{i2\pi u x/\lambda} dx$$

where $b_n(u,r) = |d_n(u,r)|^2$ and we obtain

$$b_b(u,r) = \frac{\pi r}{k}\left[\left(C(h_+) - C(h_-)\right)^2 + \left(S(h_+) - S(h_-)\right)^2\right]$$

where $k = 2\pi/\lambda$ and

$$h_\pm = \sqrt{\frac{4r}{\pi k}}\left\{\pm\frac{kL}{4r} - \frac{\pi u}{\lambda}\right\}.$$

The functions $S(x)$ and $C(x)$ are the sine and cosine integrals (Abramowitz and Stegun, (1982)) respectively. Standard numerical routines are available to evaluate these special functions (for example, Press *et al*, (1992)).

It is unlikely that the near-field expression given above will be a precise approximation to the near-field behaviour of the physical transducers, but the defocussing effects should be of similar magnitude.

Klein quote -3 dB beam widths of 1° and 0.2° along-track for the 108 and 380 kHz beams, respectively. In this case the beam widths appear to refer to squared directivity functions corresponding to identical beamforming at emission and reception. The widths of the model beams, which are approximately 1.1° and 0.3° at 108 and 380 kHz respectively, correspond well with the quoted values.

2.3 *The Sea Floor, Targets and Propagation*

The primary focus of this work is the effects of towfish motion on the imaging of *targets*, principally minelike objects. Many factors influence the imaging of the targets between emission of a pulse and the reception of the echoes. *Signal* degradation occurs due to propagation losses, sea surface and volume reverberation, refraction and other sources of noise. However, none of these factors directly affects the *image* degradation due to towfish motion, which is geometrically based, so they are disregarded in the model. Similarly, the dependence of bottom backscatter strength on grazing angle is ignored. The backscatter strength of minelike objects is generally a complicated function of orientation, so targets and the bottom are represented by patches of uniform reflectivity in the model, since aspect dependencies are outside the scope of this work.

Minelike objects are represented as level with the sea floor and consequently have no shadows. Although the capability of shadow calculation was easily added to the model, it was decided that the increased numbers of options and much increased computation time associated with shadow calculations placed them outside the scope of this work.

12

2.4 The Sidescan Image

Sidescan sonars output the responses to successive pulses as parallel stripes on the display. The pixels in each stripe correspond to ranges from the towfish, and the intensity of each pixel is the echo energy from a particular time bin, multiplied by a Time-Varying Gain (TVG) factor. The TVG is adjusted so that an image of a flat, evenly reflective area of sea bottom is as close as possible to uniform across the swath. The TVG for the Klein sonar is not explicitly known, so in this model, it is assumed that the TVG of the sidescan is perfect, and compensates for all propagation losses, effects due to grazing angle, and variation of the directivity function across-track.

For simplicity, signal degradation and effects due to grazing angle are ignored at all stages of the model. Since the TVG should negate effects due to the change in the beam profile across-track, this is normally also neglected, that is, $b_k(v)$ is set to unity. The exception to this occurs when the towfish is twisted about its cylindrical axis (rolling motion), when $b_k(v)$ must be included in the model.

One further correction included in the model is a normalisation of the directivity function with range, so that at any range, the peak value of the beam is unity. This removes the effects of defocussing in the near field from intermediate stages of the calculations. If this correction is not included, the intermediate sections of the calculation appear to show a fall-off in energy close to the towfish track, in the region where the beam is near-field defocussed and has no single intense peak.

An artificial TVG is always necessary in the final image calculation, in order to correct for movement of the beam during reception and for quantisation and normalisation effects in the calculation. The TVG function is calculated for stable motion above an evenly reflective bottom, and is used for all cases of towfish motion, since the sidescan has no knowledge of such motions.

The numerical model used to simulate the sidescan images is described in Section 4.

3. Treatment of Towfish Motion

In this study, towfish motions refer to fluctuations of the towfish position and orientation away from the ideal level, straight tow path at uniform velocity. Each towfish motion is modelled as a deterministic, sinusoidal perturbation with the general form

$$A \sin(\omega t + \phi).$$

Other motions which are not treated in this model are systematic drifts of the towfish due to currents or the towing ship changing course, and randomly changing perturbations and transients. Over short periods of time, it is expected that the generally random motion of a towfish might be approximated by a single sinusoid, since in general the driving motions of the ship and water body are approximately periodic. For simplicity, each of the individual translations and rotations was simulated separately, although the program does not require this.

Along with the local coordinate system of the towfish described in Figure 1, it is convenient to work in "world coordinates" attached to the sea floor. Let the world coordinate system be (X, Y, Z) in contrast to the local towfish coordinate

system (x,y,z). Let the origin of the world coordinate system be on the sea floor below the ideal position of the towfish at time $t = 0$. Thus, the ideal tow path of the towfish is $(0, h_0, V_0 t)$ in the world coordinate system, where h_0 is the expected altitude of the towfish and V_0 is the expected towing velocity. As with the towfish coordinate system, X points to port, Y points vertically upward and Z points along-track. Figure 4 shows the two coordinate systems.
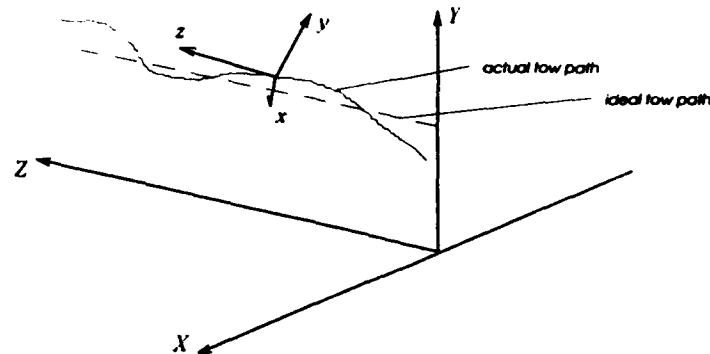

Figure 4: World coordinate system and local towfish coordinate system.

The possible motion perturbations are three rotations about the towfish origin and three translations of the towfish origin. The centres of the transducers are considered to be at the origin. The motions are known as:

1. *sway* - $\Delta X(t)$ - translation in the X direction, side to side across the track.
2. *heave* - $\Delta Y(t)$ - translation in the Y direction, up and down.
3. *surge* - $\Delta Z(t)$ - translation in the Z direction, forwards and backwards.
4. *pitch* - $\alpha(t)$ - up and down rotation in the vertical plane passing through the towfish cylindrical axis. The pitch is the angle between the towfish z-axis and the X-Z (horizontal) plane, positive when the nose points upward.
5. *yaw* - $\beta(t)$ - side to side rotation about the world Y (vertical) direction. The yaw is the angle between the vertical plane passing through the towfish z-axis and the world Z direction. Yaw is positive to port.
6. *roll* - $\gamma(t)$ - twisting rotation about the towfish z-axis. Roll is positive for anticlockwise rotation, looking forward along the axis.

Figures 5 and 6 show each of the motions in isolation. Combinations of the motions can include any of the three translations, but if multiple rotations are included, they are defined in the order: yaw *then* pitch *then* roll, in order to preserve the uniqueness of the coordinate system.

Of the six motions, three are likely to have a dominant effect on sidescan images: yaw, pitch and surge, because they cause motion of the beam along the track, in the direction in which the beam is narrow and thus most sensitive to motion. In particular, along-track motion of the beam can cause the beam to skip significant sections of the bottom. In contrast, the beam is very broad across the track, so that coverage is not reduced by a sway or heave motion.
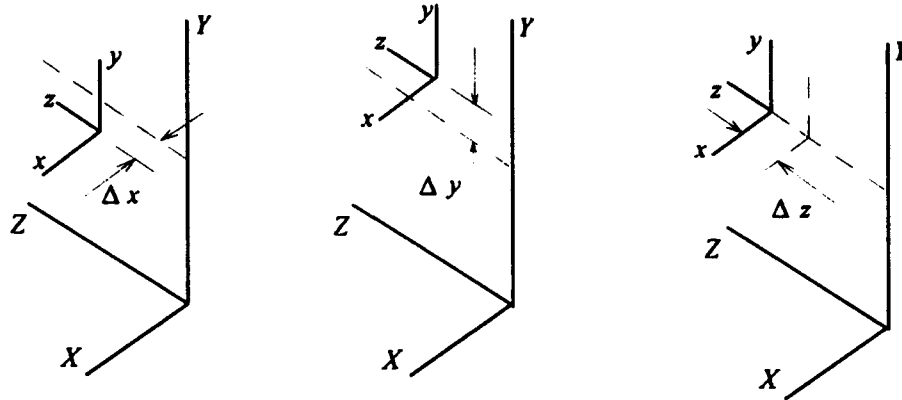
Figure 5:   *Sway (left), heave (centre) and surge (right) towfish motions.*
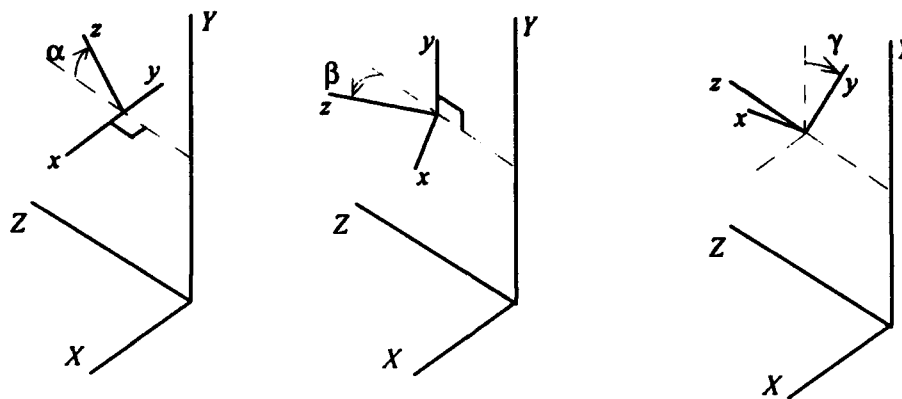
Figure 6:   *Pitch (left), yaw (centre) and roll (right) towfish motions.*

Beam directivity functions are most easily expressed in the local towfish coordinate system, so it is convenient to transform from world coordinates to towfish coordinates in order to calculate the effects of beamforming.

Let the time be t. In world coordinates, the position of the origin of the towfish is the column vector

$$\mathbf{p}(t) = \begin{bmatrix} \Delta X(t) \\ \Delta Y(t) + h_0 \\ \Delta Z(t) + V_0 t \end{bmatrix}.$$

If the *world* coordinate of a point on the sea floor is $\mathbf{q}$, then the position of $\mathbf{q}$ relative to the origin of the towfish is $\mathbf{q} - \mathbf{p}(t)$. If the axes of the towfish are subject to a single one of the rotations α, β or γ defined above, then the position $\mathbf{q}'(t)$ of the point on the sea floor relative to the *towfish* coordinate system can be represented by

---

15

$$q'(t) = T(t)\{q - p(t)\} \equiv \begin{bmatrix} x' \\ y' \\ z' \end{bmatrix}$$

where the transformations T for single rotations are defined by

$$\begin{bmatrix} 1 & 0 & 0 \\ 0 & \cos\alpha & -\sin\alpha \\ 0 & \sin\alpha & \cos\alpha \end{bmatrix}, \begin{bmatrix} \cos\beta & 0 & -\sin\beta \\ 0 & 1 & 0 \\ \sin\beta & 0 & \cos\beta \end{bmatrix}, \begin{bmatrix} \cos\gamma & -\sin\gamma & 0 \\ \sin\gamma & \cos\gamma & 0 \\ 0 & 0 & 1 \end{bmatrix}$$

for pitch, yaw and roll respectively.

A general transformation involving all three rotations requires an ordering convention for it to be unique. As before, performing yaw then pitch then roll transformations, we have the general transformation

$$T =$$

$$\begin{bmatrix} \cos\beta\cos\gamma + \sin\alpha\sin\beta\sin\gamma & -\cos\alpha\sin\gamma & -\sin\beta\cos\gamma + \sin\alpha\cos\beta\sin\gamma \\ \cos\beta\sin\gamma - \sin\alpha\sin\beta\cos\gamma & \cos\alpha\cos\gamma & -\sin\beta\sin\gamma - \sin\alpha\cos\beta\cos\gamma \\ \cos\alpha\sin\beta & \sin\alpha & \cos\alpha\cos\beta \end{bmatrix}.$$

Once the position of the point is known in the towfish coord'·· : system, the directivity function at that point is easily calculated. The dire⟍ ⱱity calculation requires the quantities $u = \sin\eta$ and $v = \sin\kappa$. Using the towfish-frame coordinate defined above, these are

$$u = \sin\kappa = \frac{z'}{r}$$

and

$$v = \sin\eta = \sin(\phi'' + \delta) \equiv \sin\left[\tan^{-1}\left(\frac{y'}{|x'|}\right) + \delta\right]$$

where δ is the transducer depression angle and r is the slant range to the point.

4. *The Sidescan Simulation Model*

An iterated method in three stages was chosen to simulate sidescan images. The sea bottom is represented by a finite grid of rectangles rather than a continuous surface.

The three stages, repeated for each pulse, are:

1. a calculation of the acoustic "energy" reaching each rectangle on the bottom, dependent only on the directivity function of the transducers at the moment when the pulse was emitted;
2. a calculation of the (electrical) "energy" which is the response of the transducer to the ech⁻ ⸏rom each rectangle on the bottom, and depends on

the result of stage 1, the reflectivity of the rectangle, and the directivity function of the transducers at the moment when the echo from the rectangle reaches the transducer;

3. the "image" stripe recorded by the sidescan sonar for the pulse. Each pixel in the stripe corresponds to the sum of all returns from a particular range interval, and is simulated in the model by a sum over all the rectangles whose range is closest to each range bin.

As noted above, the pulse duration is assumed to be so short that it does not affect range resolution, which is then only limited by the size of the rectangles used to represent the sea floor. Echoes from previous pulses are assumed to have no effect on the returns from subsequent pulses. It is also assumed that the transducer on each side of the towfish only senses echoes from its own side.

Let the area of sea floor to be imaged be divided into equal rectangles, each represented by its central point q_{ij}, $i = \{-N_x, -N_x + 1, ..., N_x\}$, $j = \{1, 2, ..., N_z\}$, where the i correspond to X values either side of $X = 0$ and the j correspond to values of constant Z. Let each rectangle have an associated reflectivity ρ_{ij}. Let pulsing (pinging) start at $t = t_0$, and the interval between pulses be $T_p = SW/c$, where SW is the width of the swath (which is assumed to be two-sided) and c is the acoustic velocity. Let N_p pulses be emitted at times $t_n = t_0 + nT$, $\{n = 1, 2, ..., N_p\}$. Finally, let the towfish position in world coordinates be $p(t)$ as defined in Section 3, and note that it is specified at all times.

The first step of the simulation yields the "energy" incident on each rectangle after the emission of a pulse. Effects due to propagation and grazing angle are left out, so the "energy" corresponds directly to the value of the transducer directivity function at the centre of each rectangle. Using the notation of Section 3, we have

$$E'_{ijn} = b\left(q'_{ij}(t)\right) = b\left(T(t_n)\{q_{ij} - p(t_n)\}\right)$$

where E'_{ijn} is the "energy" incident on the ijth rectangle from pulse n, $T(t_n)$ is the appropriate coordinate transformation at the emission time of the nth pulse, given pre-defined values for the towfish motions and b is the transducer directivity function. Scale factors are neglected since the results are relative rather than absolute values.

The second step of the simulation yields the (electrical) "energy" which is the response of the transducer to the echo returning from each rectangle. Since other effects are neglected, this is dependent only on the results of the first step, the reflectivity of the rectangles and the directivity function of the transducer at the moment when the echo from each rectangle returns. Shadowing calculations would also be included in this stage if the rectangles were given heights.

In order to calculate the moment when the echo from each rectangle returns, we first note that the towing velocity of the towfish is far less than the velocity of sound. Thus, it is a good approximation to say that the time when the echo returns is the emission time plus twice the travel time for the pulse to reach the reflecting rectangle. If the slant range when the pulse is emitted is

$$r_{ijn} = \left|p(t_n) - q_{ij}\right|$$

for the ijth rectangle, then the echo return time is approximately

$$t'_{ijn} = t_n + 2r_{ijn}/c \equiv t_n + \delta t_{ijn}$$

where the return-interval δ_{ijn} will be used later, and we have the relative value

$$E_{ijn}^R = \rho_{ij} b \left(\mathbf{T}(t_{ijn}') \left\{ \mathbf{q}_{ij} - \mathbf{p}(t_{ijn}') \right\} \right) E_{ijn}^I$$

where the response of the transducer is assumed linear and E_{ijn}^R is the "energy" response to the echo from the ijth rectangle after the nth pulse.

The third and final step of the simulation is the calculation of the sidescan image itself, using the results of step two. A sidescan image generally has a horizontal scale representing either the slant range or the horizontal across-track range. Pulse returns are imaged successively as parallel stripes whose pixel intensity is a linear measure of the energy received in each time bin, multiplied by the TVG. Each pixel is effectively an integration of the returns from a continuous annulus on the sea floor. The sidescan recorder has no knowledge of the motions of the towfish and must assign a position to a given return based only on the time of return and the estimated position of the towfish. A similar method is used in the simulation.

In the simulation, the sea floor is broken into discrete regions, so that returns from each rectangle must be assigned to the nearest time bin. This can lead to quantisation problems if the discrete rectangles are too coarse, and in general the calculation is a trade-off between accuracy, computer memory requirements and program execution time.

For convenience in image interpretation, horizontal across-track range rather than slant range is used to calculate pixel position in the image. The *estimated* across-track range is given by

$$X_{ijn} = \sqrt{\left(\delta_{ijn}/2c \right)^2 - h_0^2}$$

where h_0 is the expected towfish altitude and δ_{ijn} is the previously calculated echo-return time. If a heave motion is present, the actual height of the towfish can be below the expected height, and the square root may be imaginary for rectangles beneath the towfish. In addition, many sidescan displays include the water column beneath the towfish in order to reveal heave motions as a wavy line at the interface between the water column and the bottom. The compromise adopted in the simulation is to display horizontal across-track ranges, but adding an offset for the water column. Thus, the *offset* estimated horizontal across-track range is set to

$$X_{ijn} = h_0 \pm \sqrt{\left| \left(\delta_{ijn}/2c \right)^2 - h_0^2 \right|}$$

where the square root is subtracted if $\delta_{ijn}/2c < h_0$, and added otherwise. If no heave motion is present, the square root is always added.

Finally, let the simulated sidescan image be a rectangular array of pixel grey-scale values G_{kn} where the rows n correspond to pulses and hence stripes on the display, and the columns k to across-track range values. The number of columns is dictated by the available number of pixels across the display. After the results of the second step have been calculated, the values G_{kn} can be calculated by a summation of transducer responses E_{ijn}^R. After evaluating X_{ijn} for each rectangle on the sea floor, each energy response E_{ijn}^R is added to the pixel G_{kn} whose corresponding across-track range is closest to X_{ijn}.

If the raw G_{kn} values were displayed as an image, beam movement during reception, quantisation and beam normalisation effects could result in a simulated image containing spurious features. In order to avoid this, a "TVG"-type normalising function is calculated before the simulation. This involves the calculation of the raw G_{kn} values for stable motion above an evenly reflective and featureless seabed, for a single pulse ($n=0$, say). The reciprocals of the G_{k0} values are then used to normalise the G_{kn} values calculated in the simulation, and the simulated sidescan image is ready for display.

The intermediate steps of the simulation allow the extraction of figures for the energies E_{ijn}^I and E_{ijn}^R. Rather than retaining values of all rectangles from every pulse, only the maximum value over all pulses is stored for each rectangle, say E_{ij}^I and E_{ij}^R. These allow display of the incident and received beam footprint patterns on the bottom.

5.   *Measures of Distortion*

Quantities such as "recognisability" of an object in an image are almost entirely subjective, however a few calculations can be made to indicate approximate *local* qualities in an image, that is, factors involving changes between one pulse and the next. Another type of calculation uses the output of step two of the numerical sidescan simulation to estimate the coverage of the sidescan run, that is, the probability that a particular object on the bottom will be overlooked.

5.1 *Local Measures of Distortion*

Image distortion is difficult to measure theoretically, since sidescan images are considered as a whole, and large local image distortions may be tolerable in the context of an image which is otherwise undistorted. However, if a local distortion obscures an important small object, for example a mine, such a flaw in an image may be critically important. The following measures of distortion are meaningful only with respect to changes between successive pulses.

5.1.1 *Backscanning*

The most obvious measure of local distortion in a sidescan image is the presence of backscanning between one or more successive pulses. Backscanning can be caused by a large-amplitude, short period yaw, pitch or surge motion. It occurs when the footprints of successive pulses are laid down in reverse order along-track. The high rates of motion which cause backscanning can also cause a decrease in coverage due to the movement of the beam footprint between pulse emission and echo return, which is most important at the edges of the swath.

Backscanning can be recognised in a sidescan image by the reversal and/or duplication of objects on the sea floor, accompanied by magnification or reduction of their along-track dimensions. Backscanning results in the local destruction of the image, and the amplitudes and periods of yaw, pitch and surge motions sufficient to cause backscanning may be regarded as the upper limits of motion beyond which the image is distorted beyond recognition.

In the simple calculations following, the moving beam footprint is replaced by a static line representing the centre of the footprint at emission.

Assume a towfish velocity V_0, an interval between pulses T_p and a single sinusoidal towfish motion with amplitude A, angular frequency ω and phase ϕ.

If the towfish motion is a surge, the amplitude is a distance along-track. The pulse footprint line lies across-track, and at time t the line is located at

$$Z(t) = V_0 t + A \sin(\omega t + \phi).$$

The minimum along-track separation between successive footprint lines is

$$\delta Z = [Z(t + T_p) - Z(t)]_{min} = V_0 T_p - A\sqrt{2 - 2\cos\omega T_p}.$$

When the quantity δZ becomes negative, then the first pulse has leapfrogged the second and backscanning has occurred. This is true across the entire swath. Clearly, backscanning is more likely as amplitude increases. T_p is set by the range scale of the sidescan, and $V_0 T_p$ is the expected separation between beam footprints. Backscanning is also more likely as ω increases, and as $V_0 T_p$ decreases. Note that $1/\omega$ is not likely to exceed T_p, that is the interval between pulses is much smaller than typical towfish motion periods.

The same calculations apply for pitch and yaw motions, with small alterations. For a pitch motion, the amplitude is specified in radians. So long as the pitch amplitude is small, A can be replaced in the expression immediately above by Ah_0. For a yaw motion, the amplitude is again given in radians, and A can be replaced by AX, where X is the across-track horizontal range. The resulting expressions show that pitching effects increase with increasing towfish altitude, and yawing effects increase towards the edges of the swath.

5.1.2 Average Magnification

When pulse footprints on the seabed are closer together or further apart than expected, the result on the sidescan display is the reverse, an equivalent magnification or reduction of any objects imaged by the footprints.

An "average" pulse-to-pulse estimate of the image distortion is the average of the changes in along-track separation between successive footprints over all the possible values of the phase (equivalent to all time). The exact difference between the expected and actual along-track separation is given by

$$\delta = A\sin(\omega t + \phi)(\cos\omega T_p - 1) + A\cos(\omega t + \phi)\sin\omega T_p.$$

After averaging the square of this over phase ϕ, taking the square root and dividing by the normal separation, the RMS average of the fractional distortion between footprints is

$$\frac{\langle\delta\rangle}{V_0 T_p} = \frac{A\sqrt{1 - \cos\omega T_p}}{V_0 T_p}.$$

5.2 *The Probability of Non-Detection of an Object*

The output of the numerical sidescan simulation includes echo response energies from step 2, as defined at the end of Section 4. If the reflectivity of the sea floor is set to a uniform value at all points, then the response energies form a map of the sea floor showing the coverage of the beams. Any areas of the sea floor which do not produce an adequate response in the transducers represent insufficient coverage, and an object located in such an area could be overlooked in a sidescan survey.

We restrict attention to the along-track direction, since coverage in the across-track direction is normally adequate due to the large beam width across-track.

Assume that a target object has an along-track width Z_t, and that an electrical response energy greater than some trigger level must be received from *some* part of the object in order for it to register. The trigger level could be given relative to the peak energy response on the entire ensonified area. Using the maximum energy response values E_{ij}^R for the rectangles on the sea floor, we can calculate those rectangles on the sea floor which induce responses below the trigger level. A contiguous region of such rectangles in the Z direction is taken to represent a "hole" in the coverage. The size and distribution of such holes will depend on the magnitudes and periods of the three motions, yaw, pitch and surge, which can move the beam footprints along-track, together with the towing velocity.

If a hole is big enough to contain the entire target object, then there is a possibility that no sign of the object will be recorded by the sonar. If a response from some finite width of the object would be required in order for it to be noticed, then the value of Z_t can be adjusted to take account of this. For example, if an object has a size of 2 m along-track, but at least 400 mm of the object must be "seen" for it to register, then Z_t should be set to 1.6 m in the calculation.

As noted, non-detection is only possible if the size of the target is less than the size of the hole. The "margin" in which the target can be moved where it will avoid detection, is the difference between the target size Z_t and the hole size, say Z_h. In order to calculate the probability of non-detection at a particular across-track range, we can calculate the sum of the available margins coming from holes larger than the target size, and divide the total by the along-track length of the search area. That is, for a target of along-track length Z_t, the probability of non-detection ("miss") at across-track range X is

$$P_{\text{miss}}(X) = \frac{1}{L_s} \sum_{z : Z_h(X) > Z_t} [Z_h(X) - Z_t]$$

where L_s is the length of the search area, and the sum is over all holes large enough to contain the target.

Such a calculation is probably of most use when the true, randomly fluctuating motion of the towfish is known from an experimental measurement, over a long search area. This would allow a direct simulation of the sidescan run and the results of step 2 of the simulation could be used to calculate the non-detection probability. However, non-detection probability can also be calculated for the simple motions given in the sidescan runs and some representative examples are included later in the report.

6. Results from Numerical Simulations

Numerous simulations were made using the methods discussed in Section 4, coded as a Fortran program. The outputs of the program are three arrays yielding three grey-scaled images, corresponding to the three steps of the simulation method.

Although most sidescan displays include an image of the sea floor both sides of the tow path, the simulations were adapted to show only the starboard side of the output at each stage. This reduced execution time and allowed more detail to be displayed in the images.

In the first two steps of the simulation, the images output by the program correspond to the maximum energies recorded during all the pulses from each individual rectangular area on the sea floor. The third image is a simulated sidescan image. The program was set to include 20% margins of extra pulses at the beginning and end of the search area in order to avoid large blank areas at the ends of the first and second images, in instances of strong towfish motions. The extra pulses do not affect the third image. Most images displayed in the following sections will be of the third type. In addition, although most of the simulations were calculated at 108 and 380 kHz, only the higher resolution 380 kHz images are normally shown. This is because the effects of motion are similar at both frequencies, but the images from the lower frequency exhibit more blur, due to the larger beam width.

The factors of interest in the simulations were:

1.   coverage of the sea floor. This was judged from the output energies from the second stage of the simulation and from the simulated sidescan image.
2.   distortion, translation and backscanning of the sidescan output. This was judged from the simulated sidescan image.

Two extreme sea floor models were used in the simulations, one evenly reflective and featureless, the "blank" sea floor, the other a completely unreflective sea floor with an array of evenly-spaced reflective target objects on it, the "target" sea floor. The "blank" sea floor was used to reveal effects of towfish motions on bottom coverage, and the appearance of distinctive general features in towfish images. The "target" sea floor was used to display object distortions. More subtle effects such as loss of contrast due to towfish motions were not investigated.

The "targets" are a selection of flat objects with minelike dimensions, and features revealing image resolution. The objects are laid in lines across the track, and spaced 8 m apart. The lines of targets are spaced 5 m apart along-track. A plan view of the targets on the sea floor is effectively shown in Figure 8, mentioned in the following Section 6.2. Figure 8 is the energy response of the 108 kHz transducers due to each point on the sea bed, that is, the second output of the simulation, for an ideal, unperturbed towfish motion. Because the bottom coverage for such a motion is very uniform and without gaps, the targets are well outlined on the bottom. The five types of targets are:

1.   squares, side length 0.4 m;
2.   letter "E"s, contained in squares of side length 1 m. Each line segment comprising the letter is 0.2 m wide;
3.   minelike rectangles, 2 m long and 0.5 m wide, laid across-track;

4. letter "X"s, contained in squares of 2 m side length. The letter is
    constructed from squares of side length 0.4 m, meeting at the corners;
5. minelike rectangles, as per 3, but laid along-track.

The order of targets is repeated along-track to cover the entire imaged area.

6.1 Operating Settings and Conventions

In line with current RAN practices for the Klein dual-frequency sidescan sonar,
the following operating settings were adopted in the simulations, unless otherwise
stated:

1. towing velocity is 4 knots;
2. range scale is 100 m, so the interval between pulses is 0.13 s;
3. altitude is 10 m;
4. the depression angle δ is -10°.

All grey-scaled images represent values normalised by the maximum value in
the array. Black represents the highest energy value, white the lowest and the
scale is linear. Sixteen shades of grey are nominally available, subject to the
nature of the display device.

Sinusoidal perturbing motions were always simulated with the arbitrary phase
set to zero. This was normally adequate, since several cycles were displayed,
except for very long-period motions.

Periods of towfish motion were selected in line with the assumption that towfish
motions are the result of coupling to ship and water motions. A representative
swell period is 4 to 5 s, and motion effects increase as period decreases. Thus, a
period of 3 s was used in most of the simulations. Longer periods such as 6, 9
and 12 s were used more rarely, in order to gauge the effect of the rate of motion
on image degradation.

Except for the case of rolling towfish motion, the across-track variation of the
beam profiles is ignored, that is, the expressions used for the beam profiles are
those for linear apertures.

Each simulation comprises the record of approximately 250 pulses.

6.2 Simulations for Stable Motion

In the absence of perturbations to the motion, the remaining factors affecting the
simulated sidescan images are the beam profiles of the transducers and the
towing velocity. Resolution changes across the track because the beams are
unfocussed and diverge in the near field and the far field. There is also a large
difference in resolution between the 108 kHz beam with a 1° beam width and the
380 kHz beam with a 0.2° beam width.

At 4 knots, the separation between the centres of the footprints of successive
pulses is approximately 0.3 m. In contrast, the 1° beam widens to approximately
1.75 m at 100 m (the edge of the swath), and the 0.2° beam widens to 0.35 m.

6.2.1 108 kHz Simulations

Figures 7, 8 and 9 show the outputs of the three stages of the simulation program for stable motion at 4 knots using the 108 kHz beam.

Figure 7 shows the (maximum) values of the energies incident on the sea floor. It can be seen that virtually the entire sea floor area has the same coverage. Only the area closest to the tow path has slightly reduced coverage, due to narrowing of the beams close to the towfish. Individual beam footprints are not visible because they largely overlap. Some of the patterns visible in the figure are also due to lack of resolution in the plotting device.

Figure 8 shows the transducer response energies for the "target" sea floor with zero reflectivity except at the target objects. Coverage of the targets is almost uniform, as could be expected in perfect operating conditions.

Finally, Figure 9 shows the simulated sidescan image of the targets. Blurring of the targets due to the broadening of the beam increases toward the edge of the swath, such that features smaller than a metre are not well resolved there.

6.2.2 380 kHz Simulations

Figure 10 shows stage 3, the simulated sidescan sonar image, at 380 kHz. Clearly the resolution at 380 kHz is far better than at 108 kHz, as could be expected from the narrower beam. Only the 0.2 m wide features of the letter "E"s are not resolved correctly in the image. Note that some loss of resolution in the simulated image is due to quantisation error in the representation of the sea floor.

The results of the first two stages are much the same as Figures 7 and 8, although the coverage of the beams is not as even as for the 108 kHz simulation, since the beam width is much smaller at 380 kHz, but the along-track movement between pulses remains the same. Reductions in the 380 kHz coverage appear at intermediate across-track ranges, where the beams narrow between near-field defocussing and far-field spreading, but the effect is not severe.

Images using the 108 kHz beam do not appear again in this work, since the effects of motion on the sidescan images are similar at both frequencies, and the blurring inherent to the lower frequency complicates the effects of the motions. The other main difference between simulations of the same motion at different frequencies is a difference in bottom coverage, which occurs for yaw, surge and pitch. Coverage is discussed in the following sections where appropriate.

6.2.3 Towing velocity

An increased towing velocity can be achieved at the expense of a decrease in range scale or an increase in the along-track interval between pings. The first option has at best a neutral effect on coverage of the sea floor, however this is not likely in practice due the increased number of runs required to cover a given area and the subsequent increase in navigational errors. The second option degrades the coverage, due to gaps between the beam footprints, especially at the higher frequency. Simulations showed that at 380 kHz, an increase of velocity from 4 to 6 knots resulted in significant gaps between beam footprints, although the effect was not so important at 108 kHz.

across-track position, m
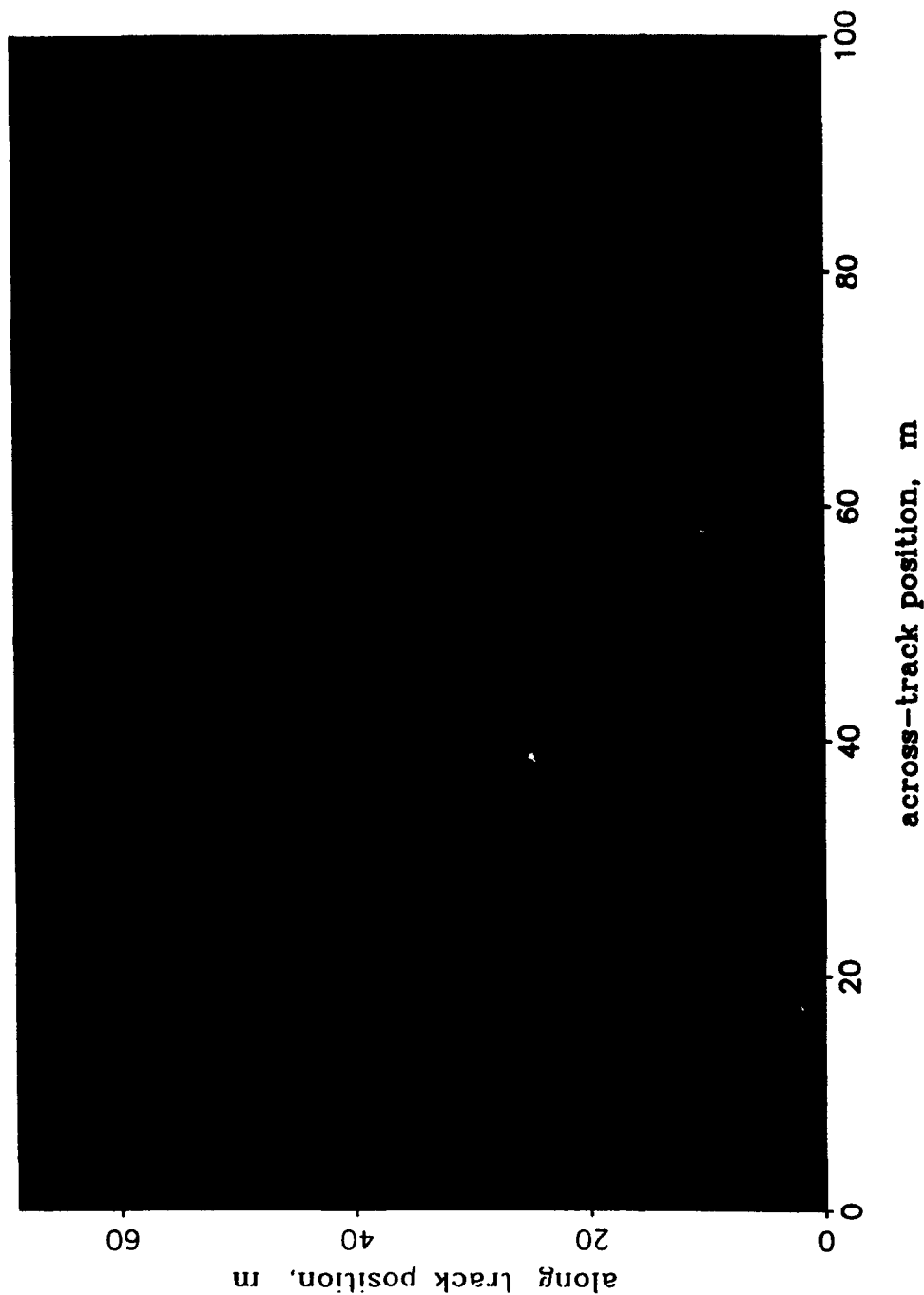
along track position, m

Figure 7: Incident energy on the sea floor: output from step 1 of the 108 kHz simulation for stable motion at 4 knots and 10 m altitude. The grey shade represents the maximum value of energy incident on each rectangle on the bottom in the course of all the pings in the sidescan run. The coverage is almost uniform, and the banding seen at the left of the image is the result of quantisation error during calculation and plotting of the image. Grey shades represent linearly scaled values, black being the maximum and white the minimum.
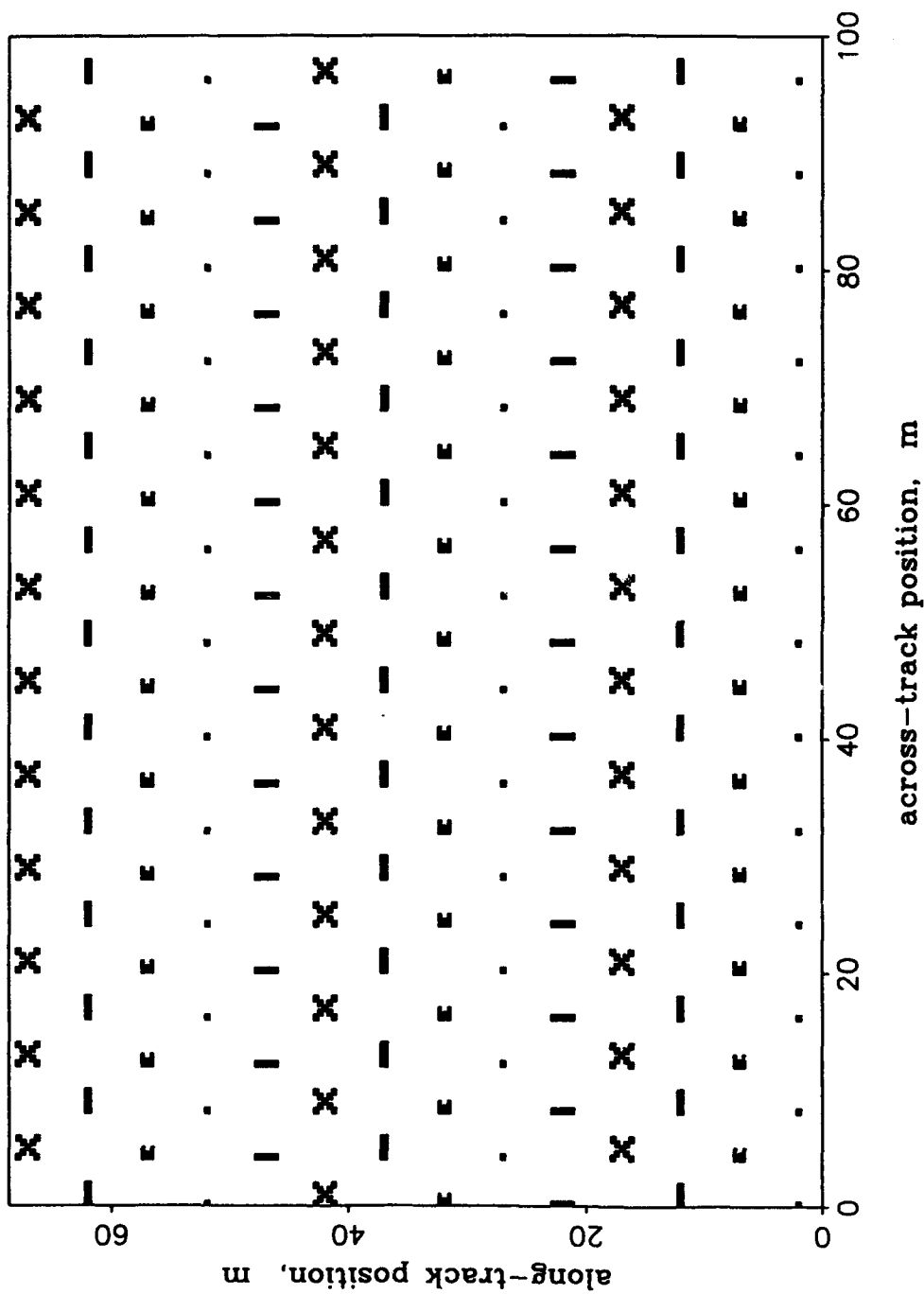
Figure 8: Energy response to echoes: output from step 2 of the 108 kHz simulation for stable motion. This represents the maximum values of transducer response energies recorded from echoes from each rectangle on the bottom after all pings in the sidescan run. The bottom is completely unreflective, except for the arrays of minelike targets shown, which are all equally reflective. Coverage is very uniform across the bottom and all the targets have produced responses in the transducer, so this is essentially a plan view of the targets.
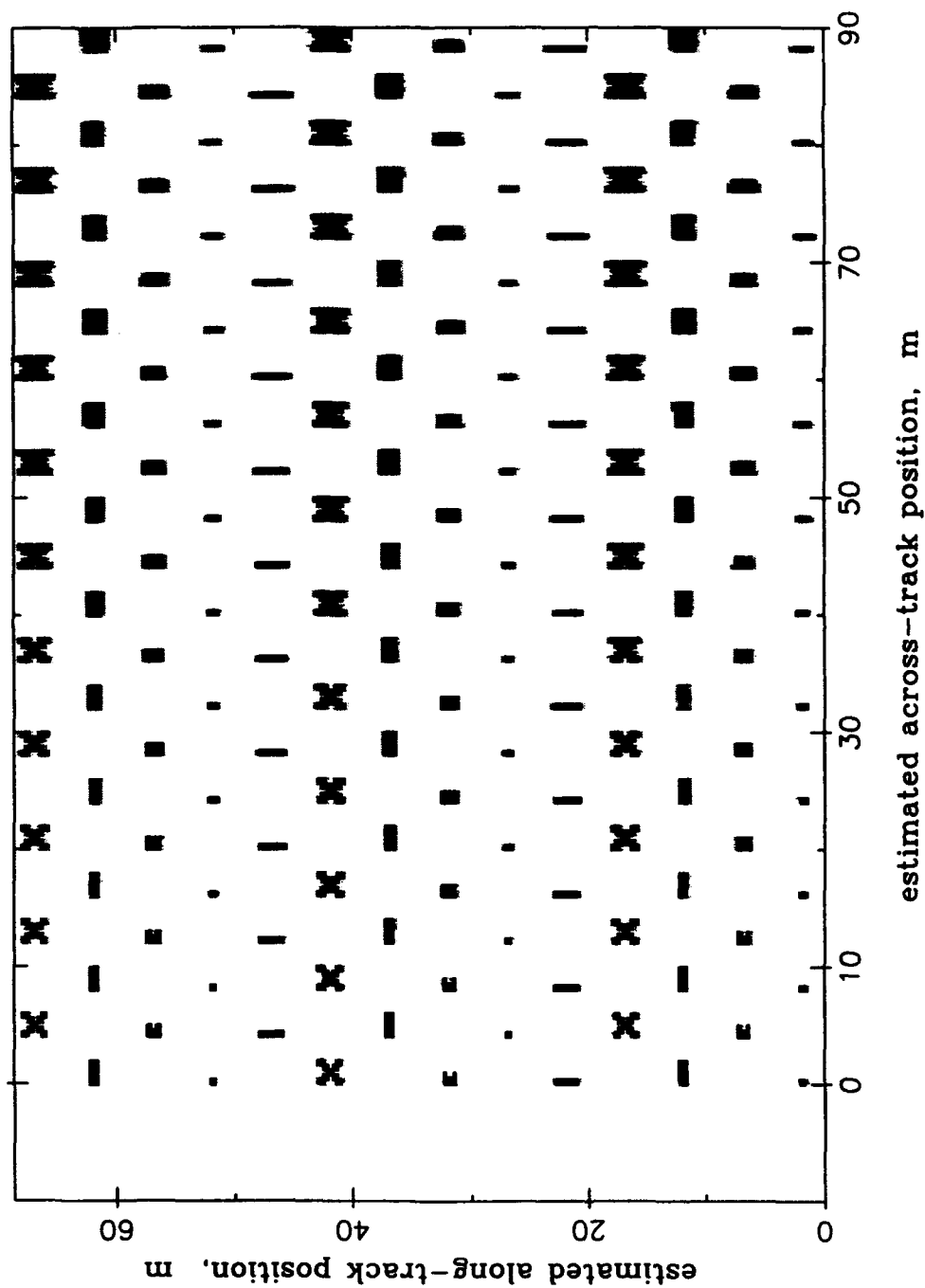
Figure 9: Simulated sidescan image of the targets: output from step 3 of the 108 kHz simulation for stable motion. The blurring seen in the image is the result of the increasing width of the beam at increasing range from the towfish. Since the altitude is 10 m, almost none of the seabed lies in the near field of the 108 kHz beam, so blurring is least nearest the tow path.

estimated across-track position, m

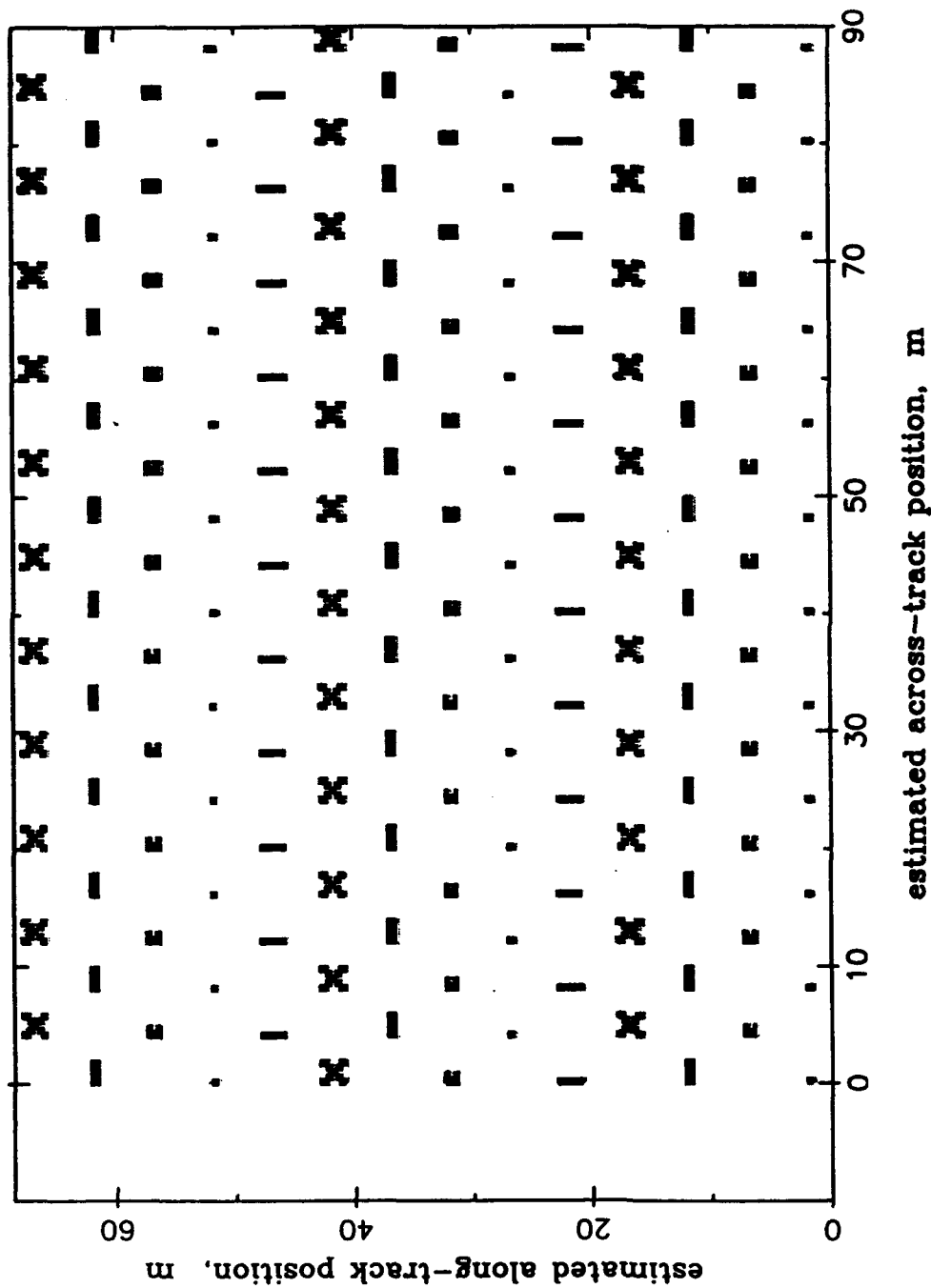estimated along-track position, m

Figure 10: Simulated 380 kHz sidescan image of the targets for stable motion, as per Figure 9. Resolution of the targets is approximately uniform across the image, since the beam width does not vary greatly. Targets at across-track ranges up to approximately 50 m lie in the near field of the 380 kHz transducer, so the beam width does not decrease in this region.

A simulation with a decreased towing velocity of 2 knots showed a marginal improvement in the resolution of the 380 kHz image, however, the improvement was not sufficient to justify halving the coverage of a sidescan survey. Only limited improvement was expected, because the beam is not focussed and consequently has a beam width only slightly less than the length of the transducers across most of the swath.

In general, it can be concluded that the nominated towing velocity of 4 knots is reasonably optimal for the Klein dual-frequency device.

6.3 Simulations for Heave Motions

Heave motions are up-and-down translations of the towfish about its normal altitude. In most cases, the sidescan can use a depth-sounder, or the time of arrival of the first bottom return, to establish the altitude. Slant ranges can then be converted to across-track ranges before display. However, if the true altitude is not known, and an assumed value is used, then the sidescan image can be affected by heave. This will also be the case if the slant range is displayed instead of the across-track range.

The effects of uncorrected heave are a shift in the apparent horizontal range of returns from a given slant range. For small magnitudes of heave, the shift in horizontal range can be approximated by

$$\Delta X \approx -h_0 \frac{\Delta Y}{|X|}$$

where h_0 is the towfish altitude, t is the heave and X is the across-track range. Thus, the effects of heave increase with altitude and decrease with horizontal range. For an altitude of 10 m, if the shift in horizontal range is to be restricted to less than 0.5 m, then the heave amplitude should be less than 0.05 times the distance across-track.

Simulations were made for a range of heave motions varying in amplitude from 0.5 to 2 m, with a period of 3 s. In line with the formula above, larger heaves distorted the image out to greater ranges, and the objects closest to the track were always distorted.

Figure 11 shows the 380 kHz simulated sidescan image of the targets for a 1 m heave with a period of 3 s. The effects are dramatic for the region directly beneath the towfish, but decrease quickly with range, becoming negligible halfway across the image. For comparison, a heave motion with 0.5 m amplitude distorts regions out to horizontal ranges of 20 to 30 m.

Coverage of the bottom is not affected significantly by heave. In general, because it is easy to correct before display, heave is the least important of the six types of motion, but if uncorrected, sidescan images should be displayed against slant range in preference to horizontal range.

6.4 Simulations for Sway Motions

Sway motions are side-to-side translations across the track. Small amplitudes of towfish sway are difficult to detect using conventional towfish location methods, and usually go uncorrected in sidescan images.
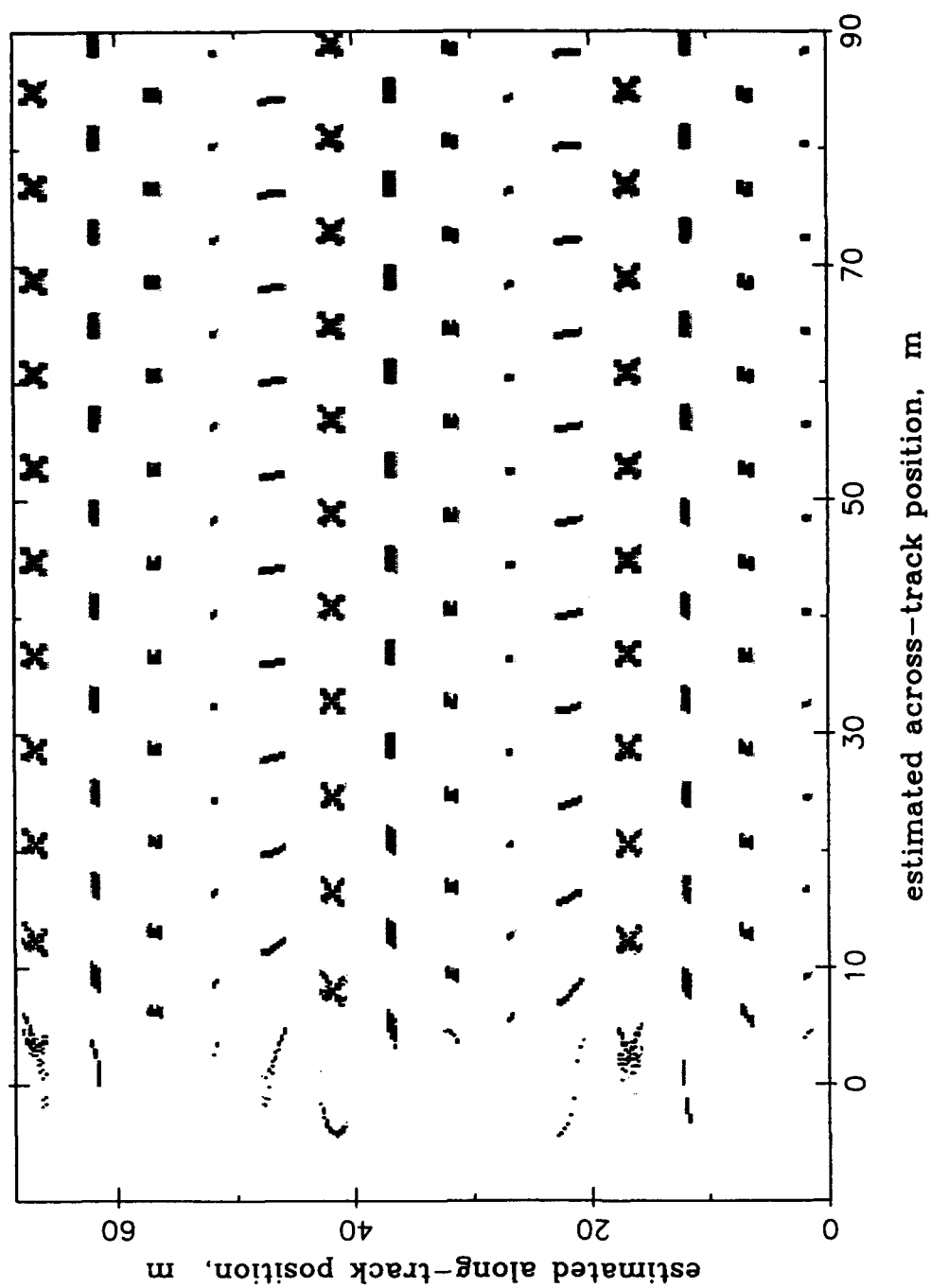
Figure 11: Simulated 380 kHz sidescan image of the targets for a sinusoidal heave motion, amplitude 1 m and period 3 s, about a towfish altitude of 10 m.

Simulations were made of a range of sway motions with amplitudes of 0.5 to 2 m, and a period of 3 s. At 0.5 m, the minelike objects were displaced, but not badly distorted. At amplitudes of 1 m and over, distortion of the objects was unacceptable. Figure 12 shows the 380 kHz simulated sidescan image of the minelike objects for a sway motion of amplitude 1 m and period 3 s. Local distortion of the objects is significant across the image.

Coverage of the bottom is not significantly affected by sway. Also it was noted that even with extremely large amplitudes of sway, objects remained recognisable due to the strong correlation between successive stripes on the image.

Cobra, Oppenheim and Jaffa (1992) and other authors cited therein, have successfully used the correlation of successive stripes on a sidescan image to remove the effects of sway. Their method was to translate each stripe across-track to maximise correlation with the preceding stripe, a technique which is easy to implement. A by-product of the technique is a more accurate positioning of the towfish.

6.5 Simulations for Roll Motions

Roll motions are twisting motions of the towfish about its cylindrical axis. The changes due to rolling motions in the positions of points on the sea floor relative to the centres of the transducers is negligible, due to the small radius of the towfish body. Thus, roll has no effect on the *positioning* of objects in a sidescan image.

The angular motion of the beam profiles must be considered relative to 40° -3 dB beam widths for both frequencies in the across-track direction. Rolls of a few degrees can be expected to have negligible effect on a sidescan image. Larger amplitudes, however, can shift the across-track beam footprint significantly, moving the peaks and nulls across-track. If the TVG function was originally adjusted to compensate for variations in the beam profile across-track, it may no longer do so when the beam has shifted, and some effect might be expected in the sidescan image.

Simulations were made for rolling motions with amplitudes from 5° to 20° with a period of 3 s. The depression angle δ of the beams was -10°. Due to the approximations in the model, particularly the use of the beam pattern of a rectangular piston, the effects noted due to across-track nulls in the beam are likely to be only qualitative.

Some decrease in the coverage of the beams close to the towfish occurred for a 10° roll. Obvious effects appeared at the centre and edges of the swath for a 20° roll. Figure 13 shows the 380 kHz simulated sidescan image of the targets for a 10° roll with a period of 3 s. Note that the targets have not shifted position, but some of the objects are fainter than others. Simulations of both sides of the swath also showed that the image was darker on the side of the swath corresponding to the transducer rotating towards the bottom.

Rolling motions of extreme amplitude may be rare, but the effects of roll are relatively independent of the period. The same effects should occur if the towfish assumed a constant list to one side, making one side of the image consistently darker than the other.
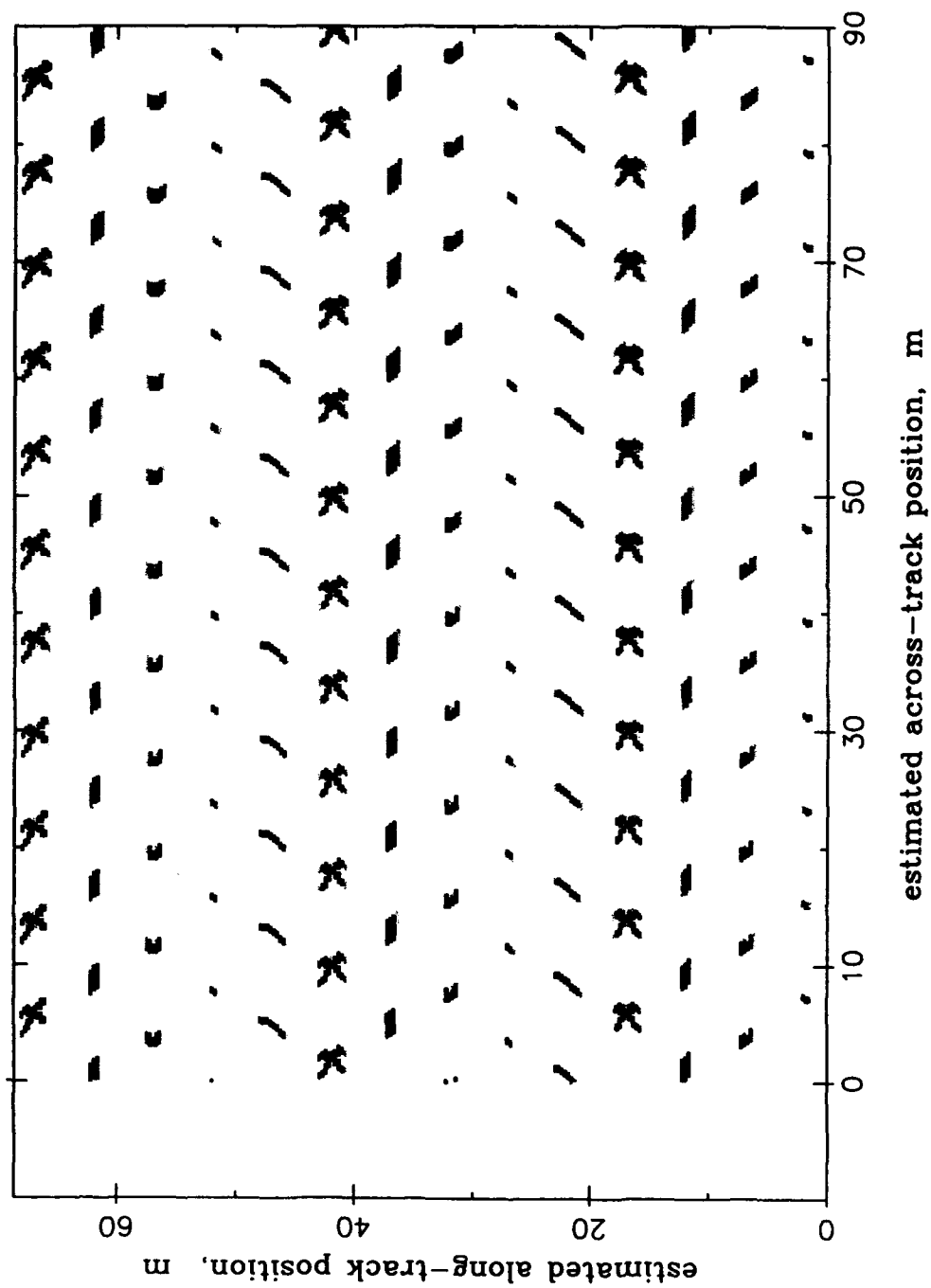
Figure 12: Simulated 380 kHz sidescan image of the targets for a sinusoidal sway motion, amplitude 1 m and period 3 s, with a towfish altitude of 10 m.
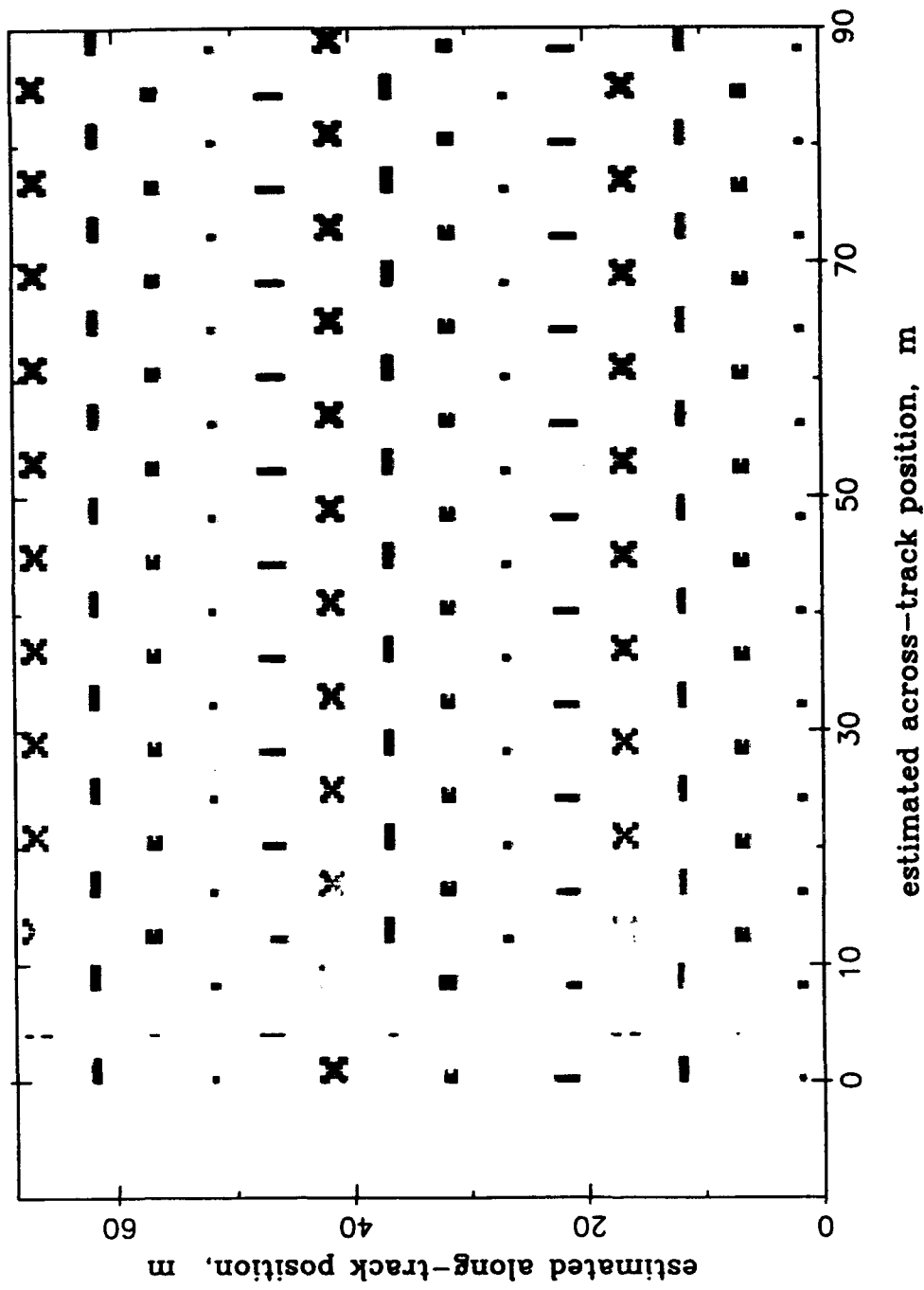
Figure 13: Simulated 380 kHz sidescan image of the targets for a sinusoidal roll motion, amplitude 10° and period 3 s, with a towfish altitude of 10 m.

33

6.6 Simulations for pitch and surge motions

Pitch and surge motions have similar effects on sidescan images, since both cause the beam footprints to move forward and backward along-track relative to their expected positions. Pitching motions are up-and-down rotations of the nose and tail of the towfish about the centre of mass. Surging motions are back-and-forward translations of the towfish in addition to the normal motion along-track.

The translation of the beam footprint along the bottom due to pitching is proportional, for small amplitudes, to the altitude h of the towfish. Pitch and surge motions affect sidescan images almost exactly the same way. Only pitch images are shown here.

Pitching/surging motions introduce the possibility of backscanning, as was discussed in Section 5.1.1. In conjunction with backscanning, a reduction in bottom coverage is to be expected because of movement of beam footprints between pulse emission and echo reception, and because the footprints will periodically be widely spaced when the footprint is moving more rapidly than its expected uniform velocity.

Simulations of pitching motions were made for amplitudes from 0.5° to 12° and periods from 3 to 12 s. Altitude was set to 10 m. Equivalent surge amplitudes are from approximately 0.1 m to 2 m.

The main effects of pitch/surge motions are magnification and reduction of the along-track dimensions of objects, due to footprints falling closer together and further apart respectively, than expected.

Noticeable magnification of minelike objects occurred for a pitch amplitude of 3° with a period of three seconds, equivalent to a 0.5 m surge. Figure 14 shows the 380 kHz simulated sidescan image of the targets for a 3° amplitude. Distortion increases rapidly for multiples of 3° amplitude.

Bottom coverage at 380 kHz is not affected for a 3° pitch, but a noticeable degradation of coverage towards the edges of the swath becomes evident for pitch amplitudes of 6° and over, with a period of 3 s. The degradation means that objects towards the edge of the swath are fainter than those near the tow path.

Bottom coverage at 108 kHz is much less affected by pitching motions, due to the increased width of the beam, which means that a much larger relative motion between the footprints at emission and beam reception is required before coverage degrades. A simulation at 9° amplitude with a period of 3 s showed only marginal decrease in coverage, and this occurred near the centre of the swath, where the beam is narrowest, rather than more toward the edges, as was the case for the 380 kHz simulations. In spite of the better quality of bottom coverage, the 108 kHz sidescan image was little improved over the 380 kHz image, since the same magnitude of distortion degraded both images.

Backscanning effects became evident at both frequencies for amplitudes of approximately 9° with a period of 3 s, equivalent to a 1.5 m surge, and obvious for a 12° pitch with a 3 s period. Figure 15 shows the 380 kHz simulated sidescan image of the minelike objects for a 12° pitch with a 3 s period. Backscanning is evident in many places where objects are duplicated and distorted. In general, the objects are also translated along-track, magnified or diminished and subject to a heave-like effect close to the towfish. Bottom coverage has diminished across much of the image, with many of the objects registering only faintly on the image. The heave-like effect results from the increase in slant range of objects at the same across-track distance but greater along-track offset, as pitch angle increases. Such effects are not observed for surge motions.

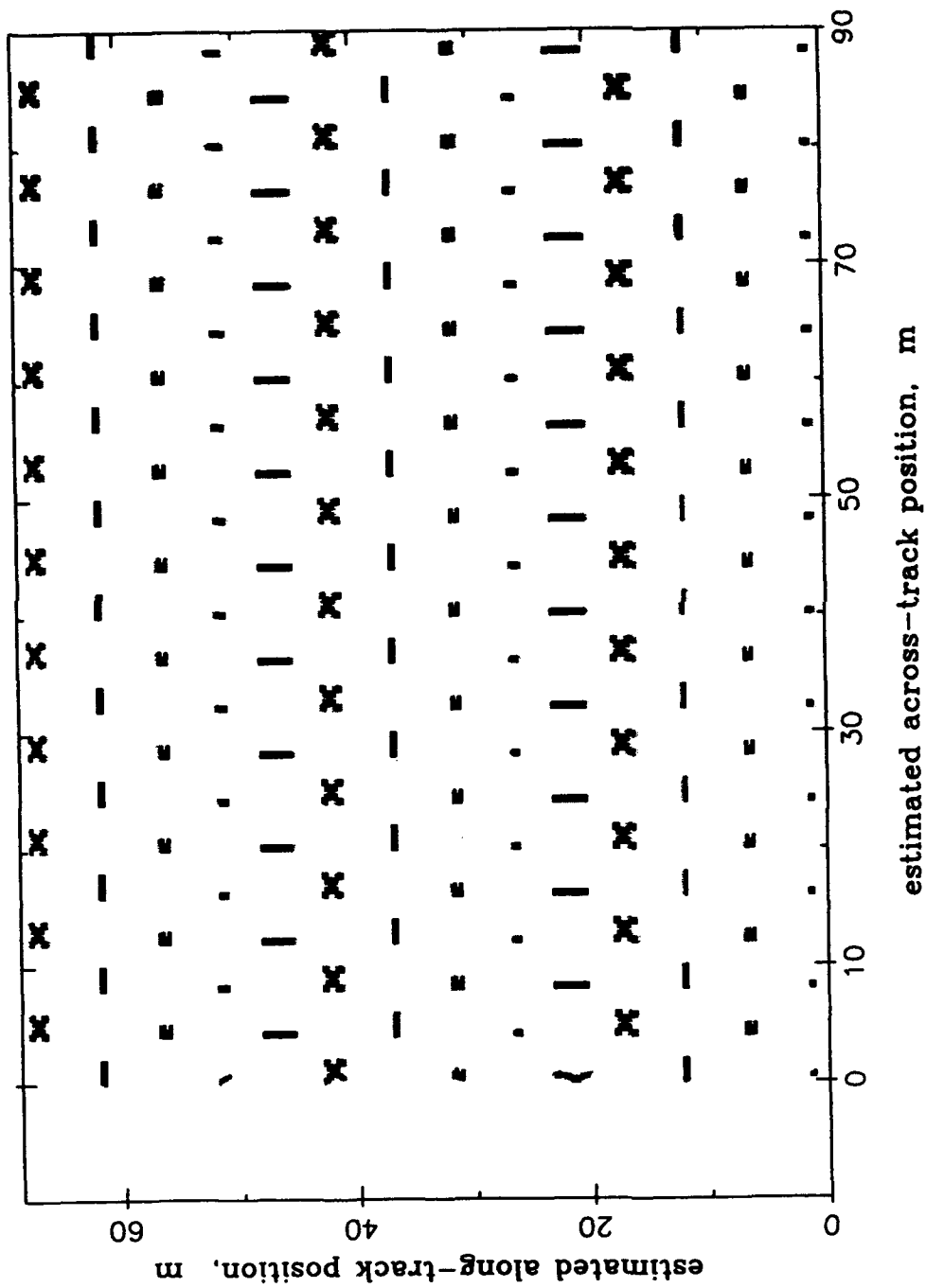*Figure 14: Simulated 380 kHz sidescan image of the targets for a sinusoidal pitch motion, amplitude 3° and period 3 s, with a towfish altitude of 10 m.*
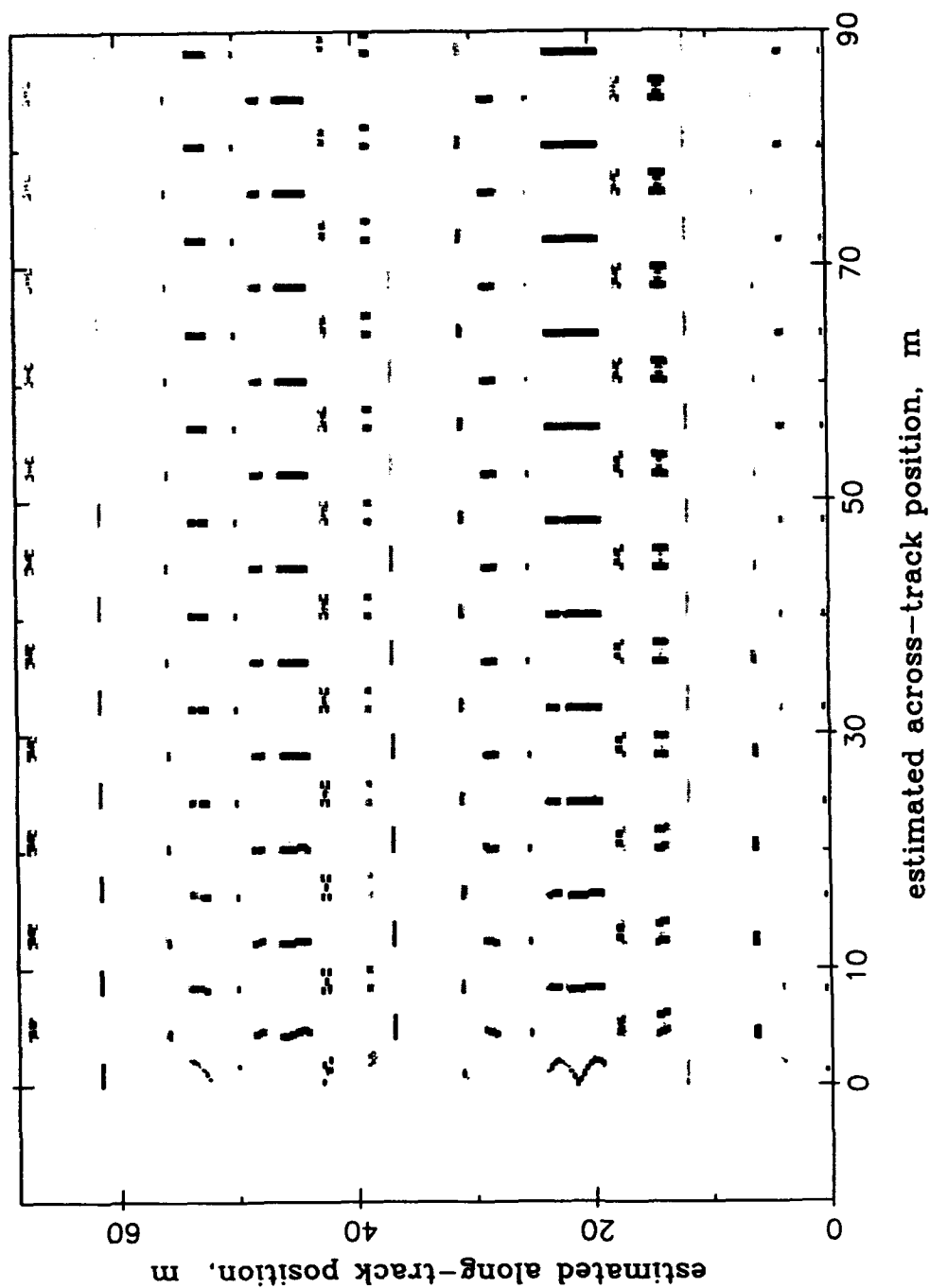
Figure 15: Simulated 380 kHz sidescan image of the targets for a sinusoidal pitch motion, as per Figure 14, but with amplitude 12°. Backscanning is visible in the image where targets are duplicated and displaced, as well as being magnified or reduced.

Simulations with longer periods than 3 s, showed that the amount of *local* image distortion is approximately inversely proportional to the period of the motion, that is, doubling the period roughly halves the pulse-to-pulse deviation of the footprint separation. However, long-period motions induce shifts of the positions of objects relative to the whole image, an effect which is obvious when amplitudes are large. A simulated sidescan image of the targets for a 12° pitch with a period of 12 s showed that backscanning had disappeared from the image, but translations of the objects remained, along with some magnification and reduction of object sizes.

Pitching and surging motions are important if their amplitudes are sufficiently large. In the case of pitching motions, the effect increases linearly with altitude. Cobra *et al* (1992) have discussed algorithms for the removal of the effects of such motions from sidescan images, and find them the hardest to identify and correct. This is not surprising, given that in the absence of diagonal lines in a sidescan image, pitch and surge effects are difficult to identify visually.

6.7 Simulations for Yaw Motions

Yawing motions are side-to-side rotations of the nose and tail of the towfish about the centre of mass. Such motions are considered to have potentially the most serious degrading effects on sidescan images, because yaw causes the beam footprint to move along-track a distance proportional to the distance across-track. For example, at the 100 m horizontal range of the edge of the swath, a 1° yaw results in a footprint translation 1.7 m along-track relative to the expected position, in contrast to an expected separation of 0.3 m between footprint centres.

Yaw simulations were made for amplitudes from 0.25° to 3° with periods from 3 to 18 s.

For a period of 3 s, significant local distortion of objects occurs for amplitudes of 0.5° and greater. Backscanning begins to occur at much smaller angles than was the case for pitch, due to the larger radius of beam motion. Backscanning occurs toward the edges of the swath for an amplitude of 1°, affecting horizontal ranges of 70 m and above, and occurs over most of the swath for a yaw amplitude of 2°, affecting ranges of approximately 40 m and above. Simulations above 3° amplitude were not carried out since the image was degraded beyond recognition at 3°.

Figures 16 and 17 show the 380 kHz simulated sidescan images of the targets for 0.5° and 2° yaw motions with 3 s periods. The 0.5° amplitude has an effect similar to blurring, but the 2° amplitude induces dramatic object magnifications and reductions, backscanning and degradation of coverage.

At 380 kHz, coverage of the bottom is degraded towards the edge of the swath for a 1° yaw with a period of 3 s, and is degraded across the image for 2° amplitude and higher. Figure 18 shows the output from step 2 of the simulation, that is, response energies, for the "blank" sea floor with a 2° yaw motion with 3 s period. At small ranges across-track, individual beam footprints can be seen. Further from the tow path, large holes appear between footprints, energies are reduced by movement of the footprint between pulse emission and echo return, and multiple backscanning occurs, where several footprints are laid down in reverse order.
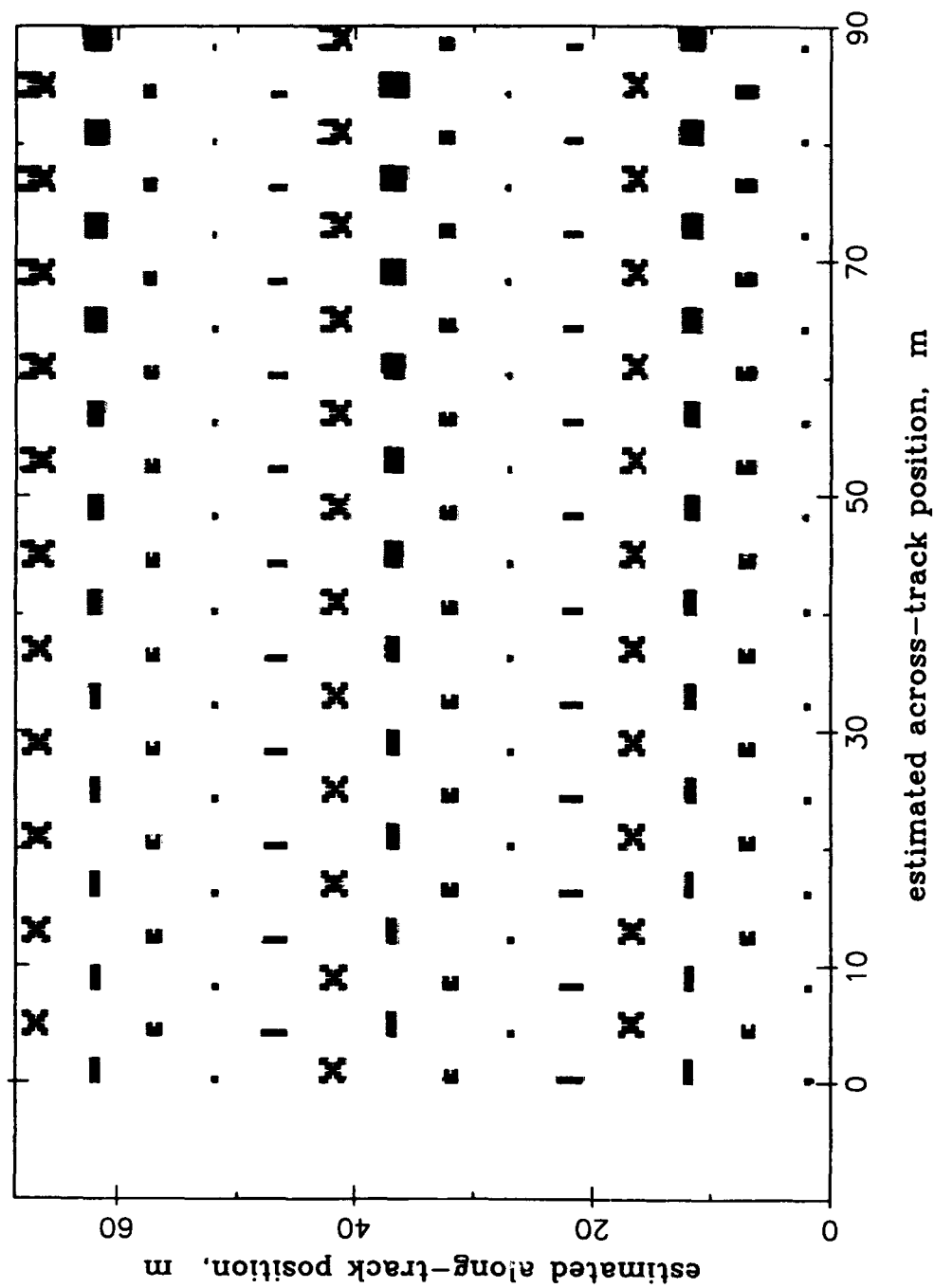
Figure 16: Simulated 380 kHz sidescan image of the targets for a sinusoidal yaw motion, amplitude 0.5° and period 3 s, with a towfish altitude of 10 m.
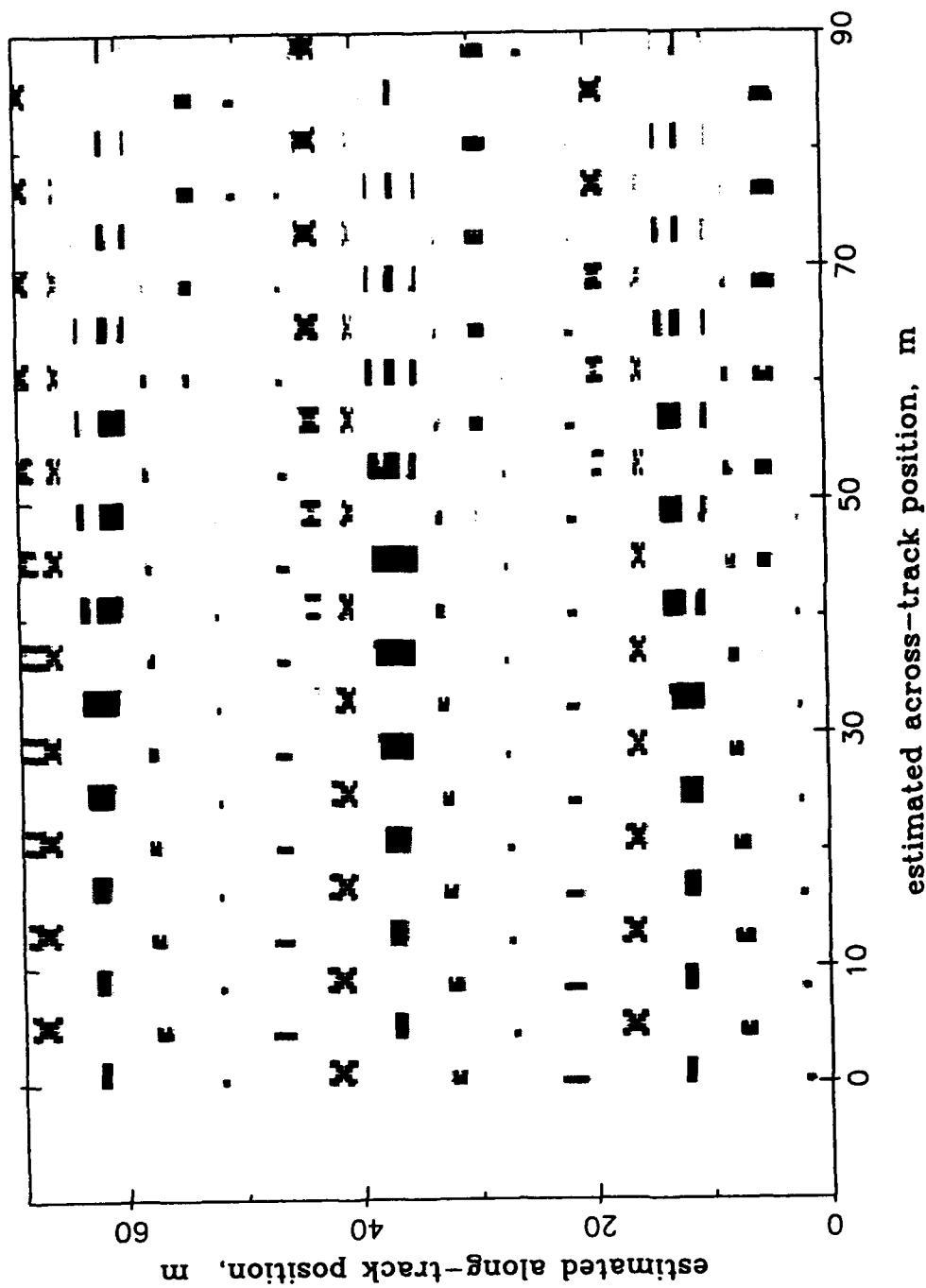
Figure 17: Simulated 380 kHz sidescan image of the targets for a sinusoidal yaw motion, amplitude 2° and period 3 s, with a towfish altitude of 10 m. Backscanning is visible in the image for across-track ranges of 30 m and above.

39
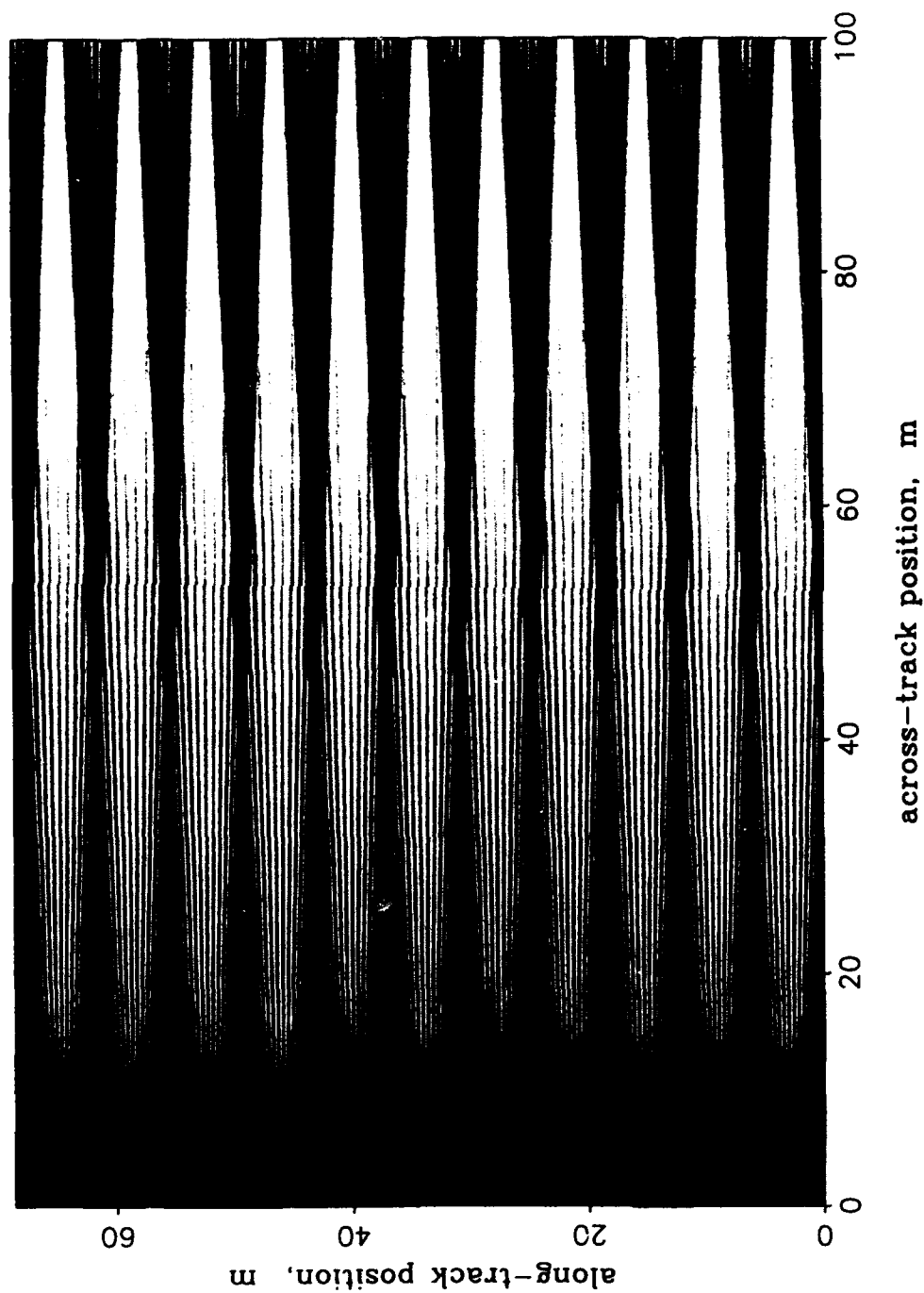
Figure 18: Energy response to echoes: output of step 2 of a 380 kHz sidescan simulation for a sinusoidal yaw motion, amplitude 2° and period 3 s, with a towfish altitude of 10 m. The seabed is uniformly reflective and featureless, so the features shown are the result of beam motion. Individual beam footprints can be distinguished in the image, and backscanned areas correspond to crossing of the footprints. Areas of the seabed with decreased coverage can be seen as pale or white areas in the image.

At 108 kHz, coverage of the bottom was relatively unaffected by amplitudes of yaw up to 3° with a 3 s period, similar to the result obtained for pitch and surge. However, the amplitudes at which distortion occurred were the same as for the 380 kHz simulations, so that the improved bottom coverage offered no advantage in the case of a yawing motion.

As with pitch, the local effects of yaw decrease approximately proportionally to the increase in period, although large-scale translations of objects remain for long-period motions. A simulated sidescan image of the targets for a 3° yaw motion with a period of 18 s, roughly equivalent to a local distortion of 0.5° yaw with a period of 3 s, showed that backscanning had disappeared from the image and coverage of the bottom was improved, but the objects remained translated out of position and were either magnified or diminished toward the edge of the swath.

In the absence of backscanning, Cobra *et al* (1992) have shown that the effects of yaw can often be successfully corrected in a sidescan image using the correlation between successive stripes on the image. Some correction is also possible if backscanned areas are identified manually and isolated from the calculation. For amplitudes of yaw large enough to degrade coverage of the bottom, such algorithms would probably fail, regardless of intervention.

In general, it appears that of the motions, it is most important to suppress short-period yaw motion wherever possible.

6.8 Analytical Checks

The simple indicators of distortion mentioned in Section 5.1 can be used to give an approximate check on the results of the numerical simulations, which in the absence of errors, should be more precise.

As was noted in Section 5.1, the separation between adjacent pulse centres along-track reaches a minimum value

$$\delta Z = V_0 T_p - A\sqrt{2 - 2\cos\omega T_p}$$

where $\delta Z < 0$ indicates backscanning, and amplitude A is used for surge motions, Ah_0 for pitch motions and AX is used for yaw motions.

In the standard operating conditions, $V_0 = 2$ ms^{-1} (4 knots) and $T_p = 0.13$ s for a 100 m range-scale.

For a motion with a 3 s period, $\omega = 2\pi/3$ rads^{-1} and backscanning commences for approximately $A = 1.0$, that is, a surge amplitude of 1 m, a pitch amplitude of 5.5° at altitude 10 m, and a yaw amplitude of 0.8° at across-track range 70 m. In contrast, obvious backscanning appeared in surge images at 1.5 m amplitude, pitch images at 9° and yaw images at approximately 1° for across-track ranges of 70 m. This represents figures up to 50% higher than the predictions, however the predictions represent threshold values, rather than values where backscanning has become obvious, so there is reasonable agreement between the two sets of numbers.

For a motion with a 12 s period, backscanning commences for approximately $A = 3.8$, that is, the threshold has increased nearly 4 times, proportional to the increase in period. This is in line with observations made in the simulations, that the locally distorting effects of motions were approximately inversely proportional to the period of the motion.

We can also use the RMS estimate of the fractional change in the distance between footprint centres, given in Section 5.1 as:

$$\frac{A\sqrt{1-\cos\omega T_p}}{V_0 T_p}$$

to estimate the amplitude for a given typical distortion. It is assumed that an unacceptable pulse-to-pulse distortion is 50%, and that the towing velocity and pulse interval have the same values as previously.

If the motion period is 3 s, then we obtain $A = 0.7$, that is, surge amplitude 0.7 m, pitch amplitude 4° at altitude 10 m, or yaw amplitude 0.6° at across-track range 70 m. Again, these values are close to the estimates of 0.5 m surge, 3° pitch and 0.5° yaw motions found to be unacceptable using the simulation program.

6.9 Non-detection Probabilities

A method for estimation of the probability of target non-detection was mentioned in Section 5.2 above, using the outputs of step 2 of the simulation program. Three of the motions, heave, sway and roll, are likely to have no effect on such a measure, since they cause little or no degradation of bottom coverage, except at extreme amplitudes.

Non-detection requires that a "hole" in the bottom coverage along-track is created by a towfish motion. This can occur either directly, when successive pulse footprints are separated by a large distance, or indirectly when movement between pulse emission and echo return decreases the response of the transducers to echoes from the bottom. Both of these effects occur most easily for yaw, rather than pitch or surge motions.

The following results are based on subjective estimates of what constitutes a "miss" and serve mainly to demonstrate the technique. A more accurate result would require experiment and more knowledge of system settings. Non-detection is taken to occur when the response falls 6 dB below the normal (ideal conditions) response amplitude in the search area. In practice, the figure would depend strongly on the nature of the seabed surrounding a target.

Figure 19 shows non-detection probabilities at 380 kHz for a pitch amplitude of 12° with a 3 s period, given a towfish altitude of 10 m. Probability levels are represented by colours: non-detection probabilities of 0, 10%, 20%... to 60% are represented by white, red, orange, yellow, green, light blue and dark blue respectively. Along-track target sizes from 0 to 2 m are shown, increasing in steps of 0.2 m. As expected, non-detection probability increases for smaller objects. Probabilities are low near the towfish due to near-field defocussing and broadening of the beam. Similarly, they decrease at the edge of the swath due to far-field spreading. A similar calculation for a 108 kHz simulation shows a far lower probability of non-detection due to the much broader beam.

A similar plot for a 3° pitch with a 3 s period shows virtually no chance of non-detection for an object of any size.
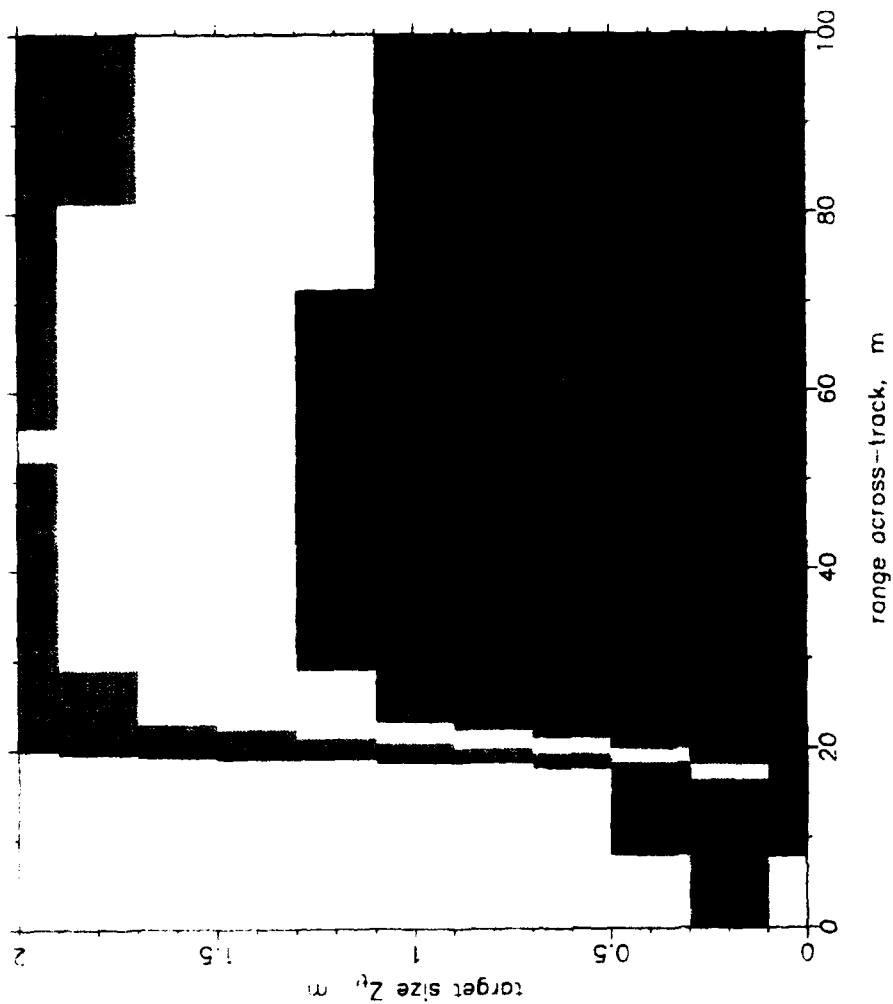
Figure 19: *Non-detection probabilities calculated from step 2 of a sidescan simulation with a sinusoidal pitch motion of amplitude 12° and period 3 s. The colours white, red, orange, yellow, green, light blue and dark blue represent non-detection probabilities up to 0, 10%, 20% ...... 60% respectively for target sizes from 0 to 2 m in steps of 20 cm. Non-detection corresponded to none of the target inducing a response above -6 dB relative to the value it would have induced in stable motion.*

Figure 20 shows non-detection probabilities for a 2° yaw with a period of 3 s. Probabilities are generally higher than for a pitch motion, reaching a maximum at an across-track range corresponding to the cross-over point of the footprints due to backscanning. At larger ranges, backscanning and far-field beam spreading actually decrease the probability of non-detection, while at lesser ranges the effects of the yawing motion decrease proportionally to the range and strongly decrease the non-detection probability. As with the pitching motion, non-detection probabilities are reduced for an identical simulation at 108 kHz.

Calculations for a 0.5° yaw with 3 s period give little probability of non-detection.

7. Conclusions

Numerical simulations of the geometric effects of towfish motions on sidescan sonar images have been performed, and some qualitative limits on the magnitudes of acceptable towfish motions have been established.

Assuming that a period of 3 s is representative of a typical towfish motion, the altitude is 10 m and the other conditions of Section 6.1 hold, then limiting amplitudes for towfish motions are approximately:

1. heave amplitudes 1/20th the smallest important across-track range if slant-range correction is required;
2. sway amplitudes of 0.5 m;
3. roll amplitudes of 10°;
4. pitch amplitudes of 3° or equivalently surge amplitudes of 0.5 m;
5. yaw amplitudes of 0.5°.

The amplitude limits given above can be extrapolated to longer periods approximately proportional to the increase in period, noting however that larger-scale image distortions are always present for amplitudes double the above figures or more, whatever the period. It may be possible to increase the period of the motions significantly by a change in towfish design or towing practice.

Bottom coverage is substantially better at 108 kHz than at 380 kHz, especially for strong towfish motions. However, the geometrical distortions of the image are similar at both frequencies, so little advantage can be gained from the improvement in coverage at the lower frequency.

The very small amplitude limit for yaw motion makes yaw the most critical motion in a consideration of towfish design. In general, the relative importance of each of the motions depends on the typical amplitudes of towfish motions, which are being measured in current DSTO experiments.
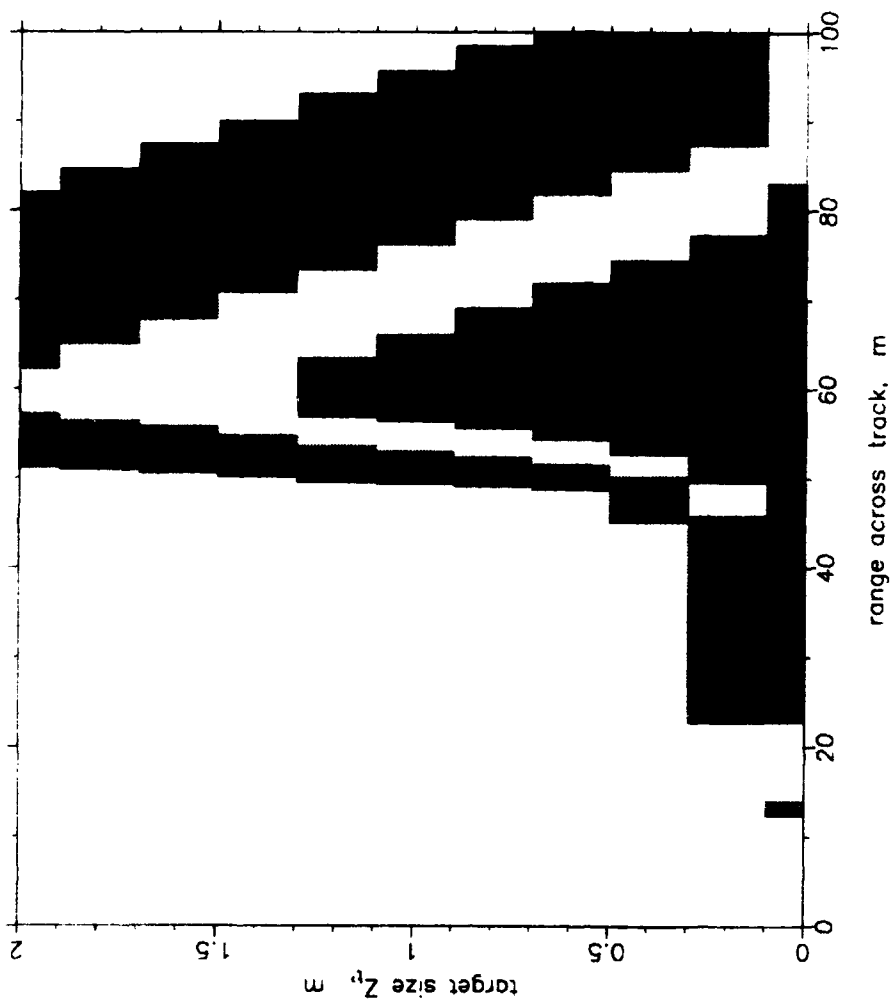
8. Acknowledgments

Figure 20: Non-detection probabilities as per Figure 19, from a simulation of a sinusoidal yaw motion with amplitude 2° and period 3 s.

9. References

Abramowitz, M. and Stegun, I., (1982)
Handbook of mathematical functions. New York: Dover

Cobra, D.T., Oppenheim, A.V. and Jaffe, J.S., (1992)
Geometric distortions in side-scan sonar images: a procedure for their estimation and correction. *IEEE Journal of Oceanic Engineering,* 17, 252-268

Press, W.H., Teukolsky, S.A., Vetterling, W.T. and Flannery, B.P., (1992)
Numerical recipes in C. Cambridge: Cambridge University Press

Ziomek, L.J., (1985)
Underwater acoustics: a linear systems theory approach. New York: Pergamon

10. Glossary of symbols

A	Amplitude
α	Pitch amplitude
b	Beam profile or directivity function for intensity
b_b	Broad beam profile - component of profile across-track
b_n	Narrow beam profile - component of profile along-track
β	Yaw amplitude
c	Sound velocity in water
δ	Depression angle of transducers
δt_{ijn}	Echo-return time interval from ijth bottom rectangle from nth pulse
δZ	Separation along-track between adjacent pulse footprint centres
ΔX	Sway amplitude
ΔY	Heave amplitude
ΔZ	Surge amplitude
E_{ij}^I	Maximum incident energy to ijth bottom rectangle from all pulses
E_{ij}^R	Maximum response energy to echoes from ijth rectangle from all pulses
E_{ijn}^I	Incident energy to ijth bottom rectangle from nth pulse
E_{ijn}^R	Response energy to the echo from ijth bottom rectangle from nth pulse
η	Across-track angle of point relative to transducer face
ϕ	Phase of towfish motion
G_{k0}	Pixel grey-scale normalisation value for kth across-track range bin
G_{kn}	Pixel grey-scale value of kth across-track range bin from nth pulse
γ	Roll amplitude
h_0	Altitude of towfish
ij	Index of rectangle on bottom
k	Index of across-track (image) range bin, (also wave number)
κ	Along-track angle of point relative to transducer face
L	Length of transducer element face
L_s	Length of search area along-track
λ	Acoustic wavelength
n	Index of pulse
N_x	Number of bottom rectangles across-track to starboard of ideal tow path

N_s	Number of bottom rectangles along-track in search area
$\mathbf{p}$	World coordinate of towfish
P_{miss}	Probability of non-detection ("miss")
$\mathbf{q}_{ij}$	World coordinate of centre of ijth bottom rectangle
$\mathbf{q}'_{ij}$	Local towfish coordinate of centre of ijth bottom rectangle
r_{ijn}	Slant range to ijth bottom rectangle at emission of nth pulse
ρ_{ij}	Reflectivity of ijth bottom rectangle
SW	Swath width (full)
t	Time
t_n	Time of emission of nth pulse
t'_{ijn}	Time of return of echo from ijth bottom rectangle from nth pulse
$\mathbf{T}$	Rotational transformation matrix from towfish to world coordinates
T_p	Duration between pings
u	Sine of along-track angle κ
v	Sine of across-track angle η
V_0	Towing velocity
W	Width of transducer element face
ω	Towfish motion radial frequency
(x,y,z)	Local towfish coordinate system (see Figure 1)
(X,Y,Z)	World coordinate system (see Figure 4)
X_{ijn}	Estimated across-track position of ijth rectangle at nth pulse
Z_h	Difference between target length and non-detection hole length
Z_t	Target length along-track

REPORT NO.	AR NO.	REPORT SECURITY CLASSIFICATION
MRL-RR-1-94	AR-008-622	Unclassified

TITLE

The effects of towfish motion on sidescan sonar images

AUTHOR(S)	CORPORATE AUTHOR
S.D. Anstee	DSTO Materials Research Laboratory PO Box 50 Ascot Vale Victoria 3032

REPORT DATE	TASK NO.	SPONSOR
February, 1994	NAV 91/165	MSPD

FILE NO.	REFERENCES	PAGES
510/207/0011	4	48

CLASSIFICATION/LIMITATION REVIEW DATE	CLASSIFICATION/RELEASE AUTHORITY
	Chief, Maritime Operations Division

SECONDARY DISTRIBUTION

Approved for public release

ANNOUNCEMENT

Announcement of this report is unlimited

KEYWORDS

Sidescan Sonar	Towfish Motion	Sonar Images
Towfish	Sonar Towfish	Image Distortion

ABSTRACT

A simulation algorithm to estimate the geometrical effects of towfish motions on sidescan sonar images is described. The results of simulations using the algorithm are discussed, and bounds for acceptable amplitudes of towfish motions are estimated. Yaw is found to be the most potentially damaging towfish motion, and a sinusoidal yaw motion with amplitude 0.5° and period 3 s is found to induce unacceptable distortion of a towfish image. The effects of towfish motions on the coverage of the seabed are also discussed.

The Effects of Towfish Motion on Sidescan Images

S.D. Anstee

(MRL-RR-1-94)

DISTRIBUTION LIST

Director, MRL - title page only
Chief, Maritime Operations Division
Research Leader, Submarine and Ship Sonar
Research Leader, Mine Warfare Operations
S.D. Anstee, MOD Sydney   9 copies
MRL Information Services

Chief Defence Scientist (for CDS, FASSP, ASSCM)   1 copy
Director (for Library), Aeronautical Research Laboratory
Head, Information Centre, Defence Intelligence Organisation
OIC Technical Reports Centre, Defence Central Library
Officer in Charge, Document Exchange Centre   8 copies
Navy Scientific Adviser
Air Force Scientific Adviser, Russell Offices
Scientific Adviser - Policy and Command
Senior Librarian, Main Library DSTOS
Librarian - MRL Sydney   5 copies
Librarian, DSD, Kingston ACT
Librarian, Australian Defence Force Academy
Serials Section (M List), Deakin University Library, Deakin University, Geelong 3217
NAPOC QWG Engineer NBCD c/- DENGRS-A, HQ Engineer Centre, Liverpool
    Military Area, NSW 2174
ABCA, Russell Offices, Canberra ACT 2600   4 copies
Head of Staff, British Defence Research and Supply Staff (Australia)
NASA Senior Scientific Representative in Australia
INSPEC: Acquisitions Section Institution of Electrical Engineers
Head Librarian, Australian Nuclear Science and Technology Organisation
Senior Librarian, Hargrave Library, Monash University
Library - Exchange Desk, National Institute of Standards and Technology, US
Acquisition Unit (DSC-EO/GO), British Library, Boston Spa, Wetherby Yorkshire LS23 7BQ, England
Library, Chemical Abstracts Reference Service
Engineering Societies Library, US
Documents Librarian, The Center for Research Libraries, US
Army Scientific Adviser, Russell Offices - data sheet only
Director General Force Development (Land) - data sheet only
DASD, APW2-1-OA2, Anzac Park West, Canberra ACT - data sheet only
SO (Science), HQ 1 Division, Milpo, Enoggera, Qld 4057 - data sheet only
Counsellor, Defence Science, Embassy of Australia - data sheet only
Counsellor, Defence Science, Australian High Commission - data sheet only
Scientific Adviser to DSTC Malaysia, c/- Defence Adviser - data sheet only
Scientific Adviser to MRDC Thailand, c/- Defence Attache - data sheet only

DISTRIBUTION LIST
(Continued)

L. Booth, MOD SYDNEY
K.E. Gross, MOD Sydney
M.W. Lawrence, MOD Sydney
G. Campanella, MOD Melbourne
R.A. Neill, MOD Melbourne
B.C. Pamias, MOD Melbourne
Mine Sweeping Project Director, Campell Park Offices CP2-3-06, Canberra, ACT
Commander, Australian Minewarfare Forces, HMAS Waterhen, Wavertton, NSW
Deputy Director, Mine Warfare Development, B-4-01, Russell Offices, ACT
Director, Minor Project Development, MHQ, Potts Point, NSW
Mine Warfare Systems Centre Project Director, Campbell Park Offices CP2-2-19,
    Canberra, ACT
OIC, Mine Warfare Operational Support Section, HMAS Waterhen, Waverton, NSW
Mine Warfare Operations Officer, HMAS Waterhen, Waverton, NSW
Mine Warfare Route Survey Officer, HMAS Waterhen, Waverton, NSW